Journal of Electroanalytical Chemistry 1015 (2026) 120171

Contents lists available at ScienceDirect

Journal of Electroanalytical Chemistry

journal homepage: www.elsevier.com/locate/jelechem

Photoelectrochemical aptasensors for tumor markers analysis: from engineered photoactive materials to sensing modes☆

Si Zhang, Zihan Huang, Jiahui Sun, Huangxian Ju *

State Key Laboratory of Analytical Chemistry for Life Science, School of Chemistry, Nanjing University, Nanjing 210023, PR China

ARTICLE INFO

Published in honor of the 80th birthday of Professor Xiurong YANG.

Keywords:
Photoelectrochemical aptasensors
Tumor markers
Photoactive materials
Sensing strategy
Signal amplification

ABSTRACT

Developing highly sensitive and accurate analytical methods to detect tumor markers can increase the likelihood of successful cure and enhance the quality of life for cancer patients. Photoelectrochemical (PEC) aptasensors have emerged as ideal analytical tools for the early diagnosis of diseases due to their advantages, including low background signal, ease of operation, low cost, and high sensitivity. In PEC biosensing photoactive materials on electrodes play a central role in converting the optical signal into electrical signal, and greatly affect the analytical sensitivity. Therefore, selecting an appropriate photoactive material is crucial for constructing PEC aptasensors, but it still remains considerable challenges. This review comprehensively outlines the latest advances in photoactive materials for constructing PEC aptasensors, emphasizes the design strategies of photoactive materials for significantly improving PEC aptasensing performance through rational engineering optical, electronic, and surface properties. The sensing modes of PEC aptasensors for tumor marker detection and the associated signal amplification strategies are classified. The latest research progress of machine learning-assisted PEC aptasensors in detecting tumor markers is also introduced. Finally, the current challenges in PEC aptasensing and future development directions are proposed.

1. Introduction

Since Edmond Becquerel's groundbreaking discovery of the photoelectric effect in 1839 [1,2], photoelectrochemistry (PEC) has been widely applied in numerous fields such as photovoltaics, photocatalysis, and PEC sensing [3–5]. The PEC process involves the conversion of photo-energy into electrical energy and the mutual conversion between electrical energy and chemical energy through charge separation and transfer of photoactive materials that absorb photons under light illumination [6,7]. PEC biosensing is an emerging technology that combines the principles of the photoelectric effect with electrochemical analysis [8–10]. It utilizes light as the excitation source, where a series of charge transfer processes occur among the analyte, photoactive materials, and electrodes, ultimately generating photocurrent signals to be detected by electrochemical instruments [11–13]. The separation between the excitation source and detection signal provides PEC sensing with high

Abbreviations: ATP, Adenosine triphosphate; AA, ascorbic acid; A1, CEA aptamer 1; Au NP-A2, Au NP labeled CEA aptamer 2; B-TiO_2 NRs, branched-TiO_2 nanorods; BDP, meso-tetra(4-carboxyphenyl)porphine; BNNS, boron nitride nanosheets; ctDNA, circulating tumor DNA; CEA, carcinoembryonic antigen; COFs, covalent organic frameworks; $[(C6)_2Ir(dcbpy)]^+PF-$ 6, (C6 coumarin-6 and dcbpy represents 4,4′-dicarboxyl-2,2′-bipyridine); CDs, carbon dots; cys-BiOBr, cysteine-induced BiOBr; Co/S-BiOBr, Co/S co-doped BiOBr; CB, conduction band; CHA, catalytic hairpin assembly; CA, captured DNA; dpMOF, dual-photosensitized MOF; 1D, one-dimensional; 2D, two-dimensional; 3D, three-dimensional; DSN, duplex-specific nuclease; dsDNA, double stranded DNA; EpCAM, epithelial cell adhesion molecule; E2, 17β-Estradiol; ET, energy transfer; E_F, Fermi level; GR, reduced graphene oxide; GSH, glutathione; g-C_3N_4, carbon nitrides; HepG2 cells, hepatocellular carcinoma cells; HPV-16, human papillomavirus-16; HCdS, hollow CdS; HCR, hybridization chain reaction; IRET, intrareticular energy transfer; LOD, limit of detection; LSPR, local surface plasmon resonance; MBD2, methyl-CpG binding domain protein 2; 5-mC, 5-methylcytosine; MOFs, metal-organic frameworks; MB, methylene blue; miRNA, microRNA; NB-g-C_3N_4/CdS, N-deficient B-doped g-C_3N_4/CdS; NFs, nanoflowers; NPs, nanoparticles; NRAs, nanorod arrays; OVs, oxygen vacancies; P5FIn, poly(5-formylindole); PTCA, perylene-3,4,9,10-tetracarboxylic acid; PEDOT, polymerized 3,4-ethylenedioxythiophene; PEC, photoelectrochemical; Pdots, polymer dots; QDs, quantum dots; R-OVs-$Bi_4O_5Br_2$, $Bi_4O_5Br_2$ with abundant oxygen vacancy defects; TE, telomerase; TNF-α, tumor necrosis factor-alpha; TBO, toluidine blue O dye; TCPP, meso-tetra (4-carboxyphenyl) porphyrin; UCNPs, upconversion nanoparticles; utg-C_3N_4, ultrathin graphite like carbon nitride; VEGF165, vascular endothelial growth factor 165; VB, valence band; WP, working photoelectrodes; ZrMOF, zirconium metal-organic framework; ZCS/TC, $Zn_{0.5}Cd_{0.5}S/Ti_3C_2$..

☆ This article is part of a Special issue entitled: 'XR YANG's Birthday' published in Journal of Electroanalytical Chemistry.

* Correspondence author.
E-mail address: hxju@nju.edu.cn (H. Ju).

https://doi.org/10.1016/j.jelechem.2026.120171
Received 12 February 2026; Received in revised form 21 April 2026; Accepted 23 April 2026
Available online 27 April 2026

sensitivity and low background noise. Additionally, by using electrochemical instruments to output signals, PEC sensing technology inherits significant advantages of traditional electrochemical detection methods, such as low cost, simple operation, fast response, and easy miniaturization [14–16]. With the continuous improvement of living standards, issues such as early cancer diagnosis, food safety, and environmental monitoring have received increasing attention. Owing to the important characteristics such as high affinity for target molecules, high specificity, high sensitivity, and secondary structural changes upon target binding, aptamers as commonly used recognition elements in PEC biosensing have made PEC aptasensors as a promising approach for tumor biomarker detection [17–20].

The detection signal of PEC aptasensors mainly originates from the photoelectric conversion process of photoactive materials [21,22]. Therefore, the rational design of photoactive materials and the regulation of charge separation and transfer within photoelectrodes are important steps in achieving high-performance PEC aptasensing [23,24]. Thanks to advances in materials science and nanotechnology, numerous photoactive materials have been developed for PEC aptasensing [25–28]. However, most single photoactive materials are limited by their light absorption efficiency and charge separation kinetics, resulting in poor PEC performance [29,30]. Consequently, it is essential to develop photoactive materials with suitable bandgap structures, high conductivity for quick charge transfer, and rapid kinetics for surface reactions. In recent years, various strategies have been employed to enhance the photoelectric conversion efficiency of PEC aptasensors, thereby improving their detection sensitivity [31–34].

Although several reviews on PEC biosensors have been published [35–39], few have focused on improving the sensing performance of PEC aptasensors by regulating the photoelectric conversion efficiency of photoactive materials. This review primarily highlights the latest research progress in regulating photoactive materials to improve PEC biosensing performance, with particular emphasis on the principles and strategies for enhancing their photoelectric performance (Fig. 1). Firstly, the development of photoactive materials, including inorganic and organic semiconductor materials, was comprehensively introduced based on the basic principles of PEC aptasensors. And several strategies to improving PEC performance and enhancing sensing sensitivity were discussed, including doping and defect engineering, morphology control, and heterostructure construction. Subsequently, recent advances in regulating PEC aptasensing modes and associated signal amplification strategies are summarized. The sensing modes are mainly categorized into signal-off mode, signal-on mode, photocurrent polarity-switching mode, and ratiometric mode. Furthermore, the research progress of machine learning-assisted PEC aptasensors in detecting tumor markers was discussed. Finally, the challenges and future prospects for improving PEC performance are outlined, offering valuable insights for researchers and practitioners dedicated to advancing the next generation of PEC sensing technologies.

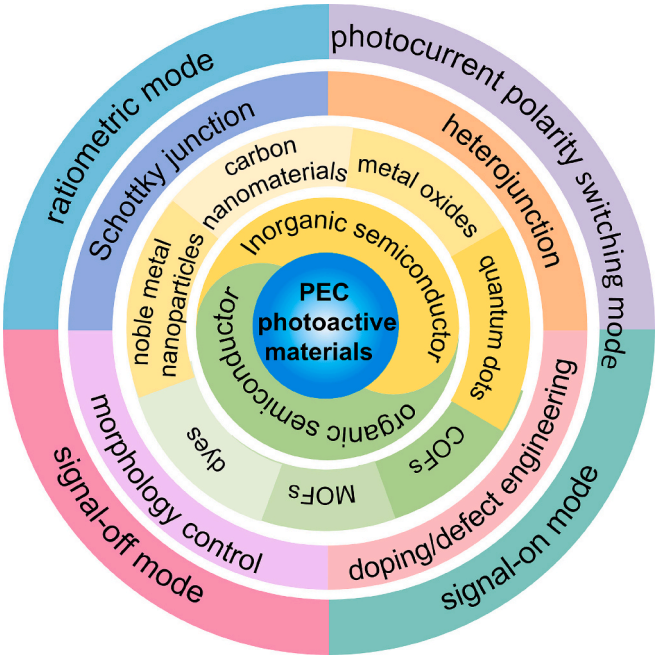

Fig. 1. Classification of photoactive materials, modification strategies, and sensing modes in PEC aptasensors, as well as their applications in tumor markers detection.

2. Principles of PEC sensing system

The commonly accepted PEC mechanisms involve three steps (Fig. 2): (i) photon absorption when photoactive materials are irradiated with light energy exceeding their band gap energy, which leads to the transition of electrons in the ground state from the valence band (VB) to the conduction band (CB) to generate electron-hole pairs; (ii) separation and transport of electron-hole pairs to the surface of photoactive materials, in which the photogenerated charge carriers may recombine to lose the energy as light or heat; and (iii) surface catalytic reactions, which generates electrical signals at the solid-liquid interface [5]. The cumulative effect of these processes determines the photoelectric conversion efficiency and the output signal intensity of the photoactive materials. The presence of the target analyte can directly or indirectly alter the environment of the photoactive material or electrolyte, causing the changes in electrical signal. Therefore, the detection signal can be modulated through various manners, providing effective approaches for the detection of different target analytes.

3. Photoactive materials

Photoactive materials, as a crucial component of PEC aptasensors, directly influence the analytical performance [40]. Generally, photoactive materials can be roughly divided into two categories based on composition: inorganic semiconductor materials and organic semiconductor materials. Specifically, inorganic semiconductor materials are further divided into three categories: quantum dots (QDs), metal oxides, carbon nanomaterials and noble metal nanoparticles. Organic semiconductor materials are further divided into three categories: dyes, metal-organic frameworks (MOFs), and covalent organic frameworks (COFs).

3.1. Inorganic PEC photoactive materials

3.1.1. Quantum dots

Since Bruce and colleagues first discovered colloidal semiconductor nanocrystals or QDs in 1983 [41,42], QDs have attracted extensive experimental and fundamental research due to their advantages, such as tunable band gaps and sizes, adjustable photoluminescence properties, broad excitation and absorption ranges, and robust photostability [43]. In 1998, Alivisatos and Nie combined QDs with specific biomolecules, opening up limitless possibilities for novel bioanalytical applications [44,45]. In 2001, Willner's group pioneered the application of quantum dot-biomolecule nanocomposites in photoelectrochemical analysis [46], ushering in a new era of fundamental research on PEC behavior of QDs and advancing the practical use of various QDs in PEC aptasensors. To date, various QDs, especially II-VI QDs such as CdS, CdSe, HgS, ZnS, and ZnSe, *etc.* [47–49], have been developed as photoactive materials. For example, Wei et al. designed a PEC aptasensor based on Br,N-codoped TiO_2 sensitized with CdS QDs for the sensitive detection of carcinoembryonic antigen (CEA, a broad-spectrum tumor biomarker) [50]. The constructed Br,N-codoped TiO_2/CdS QDs sensitization structure, featuring a narrow energy level gradient, exhibited excellent PEC

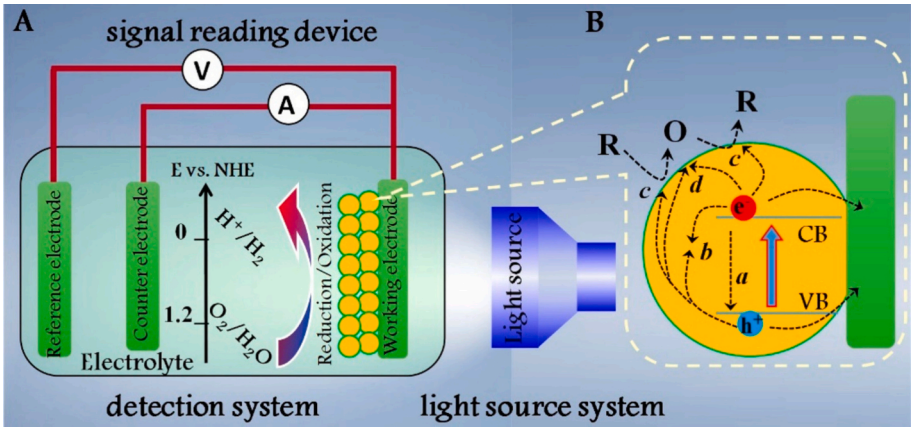

Fig. 2. (A) Diagram of the general PEC sensing system and (B) the electron-hole generation and transfer as well as possible recombination pathways. Reprinted with permission Copyright 2020 American Chemical Society [5].

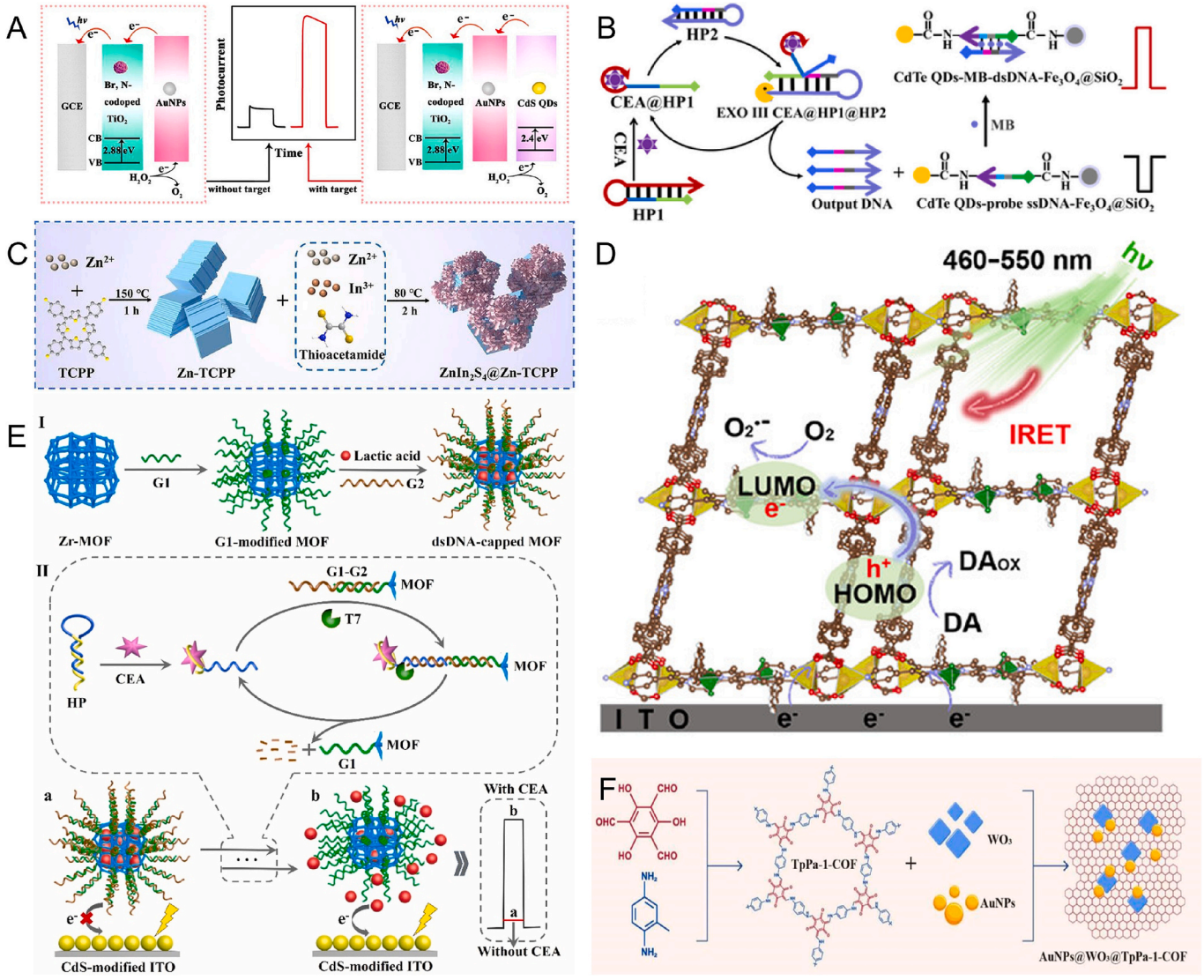

Fig. 3. (A) Mechanism of electron transfer for Br,N-codoped TiO_2 sensitized by CdS QDs. (B) Schematic diagram of polarity-switching-mode PEC aptasensing by intercalation of MB into CdTe QDs-dsDNA-Fe_3O_4@SiO_2 composites for the detection of CEA. (C) Schematic diagram of the preparation of $ZnIn_2S_4$@Zn-TCPP process. (D) Schematic diagram of the PEC process of dpMOF with IRET mechanism in the presence of dopamine and dissolved O_2. (E) Schematic diagram of the proposed PEC biosensor for CEA determination. (F) Schematic diagram of the preparation of AuNPs@WO_3@TpPa-1-COF process. Reprinted with permission Copyright 2019, 2021, and 2025 American Chemical Society [50,103,114], Copyright 2023 and 2021 Elsevier [113,115] and Copyright 2024 Springer Nature [121].

properties (Fig. 3A). With the continuous development of nanomaterials, some heavy metal-free QDs, core-shell structured QDs, ternary, or even multicomponent QDs have been studied to evaluate their potential as photoactive materials, such as black phosphorus QDs [51], SnSe QDs [52], MoS_2 QDs [53], Ag_2Se QDs [54], ZnCuInSe QDs [55], $Cs_3Bi_2Br_9$ QDs [56], $AgInS_2$/ZnS QDs [57], and $AgInSe_2$ QDs [58]. Therefore, QDs can effectively broaden the light absorption range and accelerate charge separation and transfer by sensitizing the photoelectrode, thereby improving their PEC response.

3.1.2. Metal oxides

Metal oxides exhibit semiconductor properties, and possess a wide range of applications due to their strong light-absorption capabilities, low toxicity, high chemical stability, and excellent photocatalytic activity [4,59,60]. Since Akira Fujishima and Honda first demonstrated the use of TiO_2 electrodes for photocatalytic water splitting under ultraviolet light irradiation in 1972 [61], TiO_2 has been rapidly applied in various fields, including photocatalysis, sensors, solar cells and drug delivery. In 2006, Li et al. reported the first label-free PEC strategy using TiO_2 for detecting hairpin DNA hybridization [62]. Subsequently, numerous PEC aptasensors based on metal oxides have emerged [63,64]. For example, Wei et al. utilized a TiO_2/poly (5-formylindole) (P5FIn) heterojunction as a photoactive material to construct a PEC sensor for detecting glutathione (GSH) and 17β-Estradiol (E2) (GSH and E2, a common biomarker of ovarian cancer) detection using a cascade signal amplification strategy [65]. TiO_2 and P5FIn exhibit excellent energy level matching, which promotes charge separation and transfer and provides strong and stable photocurrent signals for PEC analysis. In addition, metal oxides are generally classified into two types: n-type and p-type semiconductors. When the stoichiometric ratio is biased toward oxygen deficiency, the metal oxide materials exhibit n-type behavior, such as TiO_2, Ta_2O_5, ZnO, WO_3, SnO_2, Fe_2O_3, and In_2O_3 [66–69]. Conversely, when the stoichiometric ratio shifts toward oxygen richness, the metal oxides behave as a p-type semiconductor, such as NiO, CuO, Cu_2O, Co_3O_4, Bi_2O_3, and MoO_3 [32,70,71]. In recent years, photocathode biosensors based on p-type semiconductors have attracted widespread attention due to their excellent anti-interference properties and high stability. For instance, Li et al. employed an iridium complex-sensitized NiO photocathode for cathodic PEC detection of miRNA-122 (a key biomarker for early liver cancer diagnosis) [72]. Yang et al. synthesized an atom-shared plasmonic Bi-Bi_2O_3 hetero-nanostructure enriched with oxygen vacancies for high-performance photocathodic analysis, achieving sensitive detection of miRNA-221 aberrantly expressed in hepatocellular carcinoma [73]. This research highlighted the importance of fabricating high-performance photocathodes in PEC biosensing and encouraged further exploration of multifunctional materials for broader applications.

3.1.3. Carbon nanomaterials

Carbon is one of the most abundant elements in both inorganic and organic materials. In recent years, carbon nanomaterials have attracted increasing attention in PEC biosensing due to their inherent advantages, including excellent photostability, fast electron mobility, high biocompatibility, and a large specific surface area [74–76]. The combination of carbon nanomaterials with inorganic and organic semiconductor materials has been proven to significantly improve PEC performance, making them highly valuable for developing high-sensitivity and efficient PEC aptasensors. Carbon nanomaterials are mainly divided into carbon dots (CDs), graphene, and carbon nitrides (g-C_3N_4). CDs are nanoparticles (NPs) ranging from 1 to 10 nm in size, exhibiting unique optical and electronic properties [77–80]. Wang et al. reported that CDs as photosensitizers enhanced the photocurrent of dumbbell-shaped gold nanorods/terminal TiO_2 NPs. This enhancement was attributed to the strong visible light absorption of CDs, which broadened the TiO_2 absorption spectrum and amplified the photocurrent signal [81]. Graphene, a metal-free semiconductor, consists of a honeycomb lattice formed by layers of carbon atoms [82]. Since its successful preparation in 2004 [83,84], graphene and its derivatives have shown great potential in biosensing due to their large specific surface area, unique electronic properties, and ease of surface modification. For example, Zou et al. designed a signal on-off type PEC biosensor for the sensitive detection of CEA [85]. This sensor employed SnS_2 nanosheets on reduced graphene oxide (GR) as the photoactive material, and Au NPs coated on GR functionalized CuS to achieve signal amplification. The effective enhancement of charge transfer on the electrode by GR promoted the separation of electron-hole pairs, resulting in an enhanced photocurrent response and excellent analytical performance of the PEC detection platform. In recent years, g-C_3N_4 has attracted significant attention in PEC biosensing due to its facile preparation, environmental friendliness, excellent light-harvesting ability, and tunable energy bands [86,87]. For example, Zheng et al. developed a promising enhanced PEC biosensor for the quantitative determination of 5-methylcytosine (5-mC) (a robust diagnostic, prognostic, and predictive biomarker of cancer) based on a co-sensitization strategy and coupled with a bridged DNA nanoprobe as a capture probe [88]. The perfect match of energy level arrangement between TiO_2 and g-C_3N_4, combined with the unique optical properties of Au NPs, generated a strong photocurrent, significantly improving the detection performance of the PEC aptasensor. Bi et al. constructed a near-infrared light-driven PEC biosensor based on N-deficient B-doped g-C_3N_4/CdS (NB-g-C_3N_4/CdS) assisted by the CRISPR-Cas12a system for the detection of miRNA-21 highly expressed in most malignant tumors [89].

3.1.4. Noble metal nanoparticles

In recent years, noble metal nanoparticles have been extensively utilized as key components to enhance the sensing performance of PEC aptasensors [90,91] due to their advantages, including non-toxicity, excellent chemical stability, superior conductivity, outstanding optical transduction properties, and high specific surface area [92]. Au, Ag, Pd and Pt nanoparticles are the most popularly used noble metal nanoparticles. They are commonly used to modify various semiconductors due to their local surface plasmon resonance (LSPR) effect, which broadens the light absorption range. Additionally, noble metal nanomaterials can act as electron traps for facilitating the separation of electrons and holes, reducing charge recombination rates, and promoting rapid charge transfer kinetics, which greatly improve PEC performance [93]. For example, Wang et al. designed Nd-MOF nanorods as photoactive elements to construct a PEC platform [94]. In the presence of target vascular endothelial growth factor 165 (VEGF165, a biomarker of breast cancer, lung cancer, and lymphoma), AuNPs are introduced onto electrode surface to accelerate the charge separation of Nd-MOF nanorods due to the excellent conductivity and local surface plasmon resonance effect of AuNPs. Similarly, Qu et al. synthesized Er-MOF/AuNPs nanocomposites by integrating AuNPs on the surface of Er-MOF nanocubes [95]. AuNPs not only enhance photoelectric conversion efficiency but also provide active sites for immobilizing thiol-functionalized aptamers. Li et al. used noble metal nanoparticle labeled signal aptamers to develop a dual-wavelength responsive sandwich-type PEC aptasensor for simultaneous detection of CEA and carbohydrate antigen 153 tumor markers based on the size effect, plasmon resonance, and the response of the noble metal nanoparticle enhanced system to different excitation wavelengths [96].

3.2. Organic PEC photoactive materials

3.2.1. Dyes

Organic dyes are widely used in solar cells and PEC biosensing due to their high efficiency, ease of modification, tunable electron transfer processes, and low cost. Therefore, dye sensitization is considered as an effective method to improve photoelectric conversion efficiency in PEC systems [97,98]. Common dyes include methylene blue (MB), $[Ru(bpy)_3]^{2+}$, rhodamine B, zinc phthalocyanine, *etc.* [99–101]. For

example, Fu et al. reported a simple PEC biosensor based on an integrated cosensitization strategy and p-n heterojunction quenching for detecting miRNA-21 [102]. Due to the cosensitization effect of Bi_2S_3 and toluidine blue O dye (TBO), the photocurrent of TBO@Bi_2S_3-ZnS increased by 136 times compared to ZnS alone, demonstrating the superior visible light absorption and photoelectric conversion efficiency of TBO@Bi_2S_3-ZnS. Moreover, dyes can also serve as signal probes in PEC biosensing. For instance, a polarity-switching-mode PEC aptasensor for CEA was constructed by embedding MB in amplified double-stranded DNA connected to superparamagnetic Fe_3O_4@SiO_2 composites (Fig. 3B) [103].

3.2.2. Metal-organic frameworks

MOFs are a class of porous crystalline materials formed by the coordination of organic ligands with metal ions or clusters [104,105]. The concept of MOFs was first proposed by Yaghi et al. in 1995 [106]. MOFs exhibit several unique characteristics, including high specific surface area, tunable pore size, chemical stability, and reliable host guest interactions. These properties enable their potential applications in various fields such as gas adsorption and separation, drug delivery, catalysis, biomedical imaging, and sensing [107–109]. Furthermore, the diversity of metal centers and organic ligands, along with adjustable synthesis parameters, provides great flexibility for synthesizing MOFs with different pore sizes, structures, crystallinity, and chemical and physical properties. Importantly, MOFs can be fabricated into robust solid systems for immobilizing oligonucleotides *via* adsorption, van der Waals interactions, or covalent binding [110]. In 2012, Hou et al. reported a PEC sensor based on MOF thin films [111], advancing the development of MOFs in PEC sensing. Ju et al. designed an *in situ* release strategy for ascorbic acid (AA, an electron donor) on photoelectrodes to achieve polarity reversal of photocurrent in zirconium metal-organic frameworks (ZrMOF), enabling highly sensitive PEC detection of VEGF165 [112]. The porous structure of ZrMOF facilitates the diffusion of electron donors and increases reaction sites, thereby enhancing the electron transfer in PEC. Based on the $ZnIn_2S_4$@Zn-TCPP (TCPP: meso-tetra (4-carboxyphenyl) porphyrin) heterojunction, Du et al. developed a near-infrared light-assisted dual-modal PEC and photo-fuel-cell-driven self-powered biosensor for sensitive detection of miRNA-21 (Fig. 3C) [113]. Zn-TCPP, composed of well-isolated and evenly distributed Zn—O clusters, possesses numerous active sites and ultrathin nanosheet-like structures, exhibiting excellent PEC performance. Recently, to address the issues of narrow wavelength absorption and low photon utilization, our group designed and synthesized a dual-photosensitized MOF (dpMOF) that achieves intrareticular energy transfer (IRET) and multiple wavelength light absorption to enhance PEC performance (Fig. 3D) [114]. Specifically, the dpMOF employed the $[Cd_2(COO)_4]$ paddlewheel unit as the metal node, with meso-tetra(4-carboxyphenyl) porphine (BDP) and pyridine-functionalized boron dipyrromethene (Por) ligands serving as the energy acceptor and donor, respectively. Experimental results and theoretical calculations demonstrated that the IRET process from BDP to Por ligands within the MOF skeleton improved photon utilization and charge separation, resulting in an IRET efficiency of up to 88.3% at 545 nm and a 2.6–6.5-fold increase in photocurrent. In addition, MOFs can function as carriers for encapsulating and transporting guest molecules. For example, Li et al. developed an immobilization-free PEC biosensor based on nucleic acid-functionalized MOFs combined with a T7 exonuclease-assisted recycling process for ultrasensitive detection of CEA (Fig. 3E) [115]. In this system, MOFs efficiently encapsulated electron donors, while double-stranded DNA (dsDNA) acted as a molecular gate structure for the pores. Upon the presence of CEA, dsDNA recognition targets triggered conformational changes and T7 exonuclease-aided recycling amplification, opening the MOF pores and releasing a large number of electron donors, which significantly enhanced the photocurrent. Compared to traditional PEC biosensors that require probes to be immobilized on the photoelectrode, this biosensor avoided steric hindrance effects and improved recognition and digestion efficiency. Furthermore, Zhou et al. demonstrated methylene violet encapsulated zeolite imidazolate frame-90 and stimuli-responsive decapsulation to achieve dual-mode PEC and fluorescence bioanalysis for detecting adenosine triphosphate (ATP, which may induce cancer and cardiovascular diseases), with limits of detection (LOD) of 3.2 pM and 4.1 pM, respectively [116].

3.2.3. Covalent organic frameworks

In 2005, Yaghi, a pioneer in the development of MOFs, and his colleagues discovered a crystalline organic porous material named covalent organic frameworks [117]. COFs are formed by linking light elements (*e.g.*, C, N, H, O, B, and Si) through strong covalent bonds (*e.g.*, B—O, C—N, C═N, and C=C–N). It has unique properties, such as a periodic structural arrangement, abundant functional groups, low toxicity, tunable porosity and chemical structure, which offer great potential for developing photoactive materials for PEC aptasensors [118,119]. In 2019, Yang et al. applied COFs in a PEC aptasensor, demonstrating their considerable promise in PEC biosensing [120]. In 2024 Zheng et al. utilized AuNPs@WO_3@TpPa-1-COF as a photoactive material and designed a PEC sensing approach to detect DNA methylation (serves as a mechanism for inactivating tumor suppressor genes and activating oncogenes during tumor development) levels and multiple methylated sites [121] (Fig. 3F). More recently, Yang et al. constructed a PEC biosensor for detecting circSATB2 (a biomarker for early cancer diagnosis) based on CRISPR/Cas13a-programmed Cu nanoclusters and a *Z*-scheme T-COF/Ag_2S composite [122]. The COF films grown *in situ* on the photoelectrode surface can accelerate charge transfer between the photoelectrode and the COF interface, thereby improving the stability and detection accuracy of PEC aptasensors. Although many COFs have been applied in gas storage and photocatalysis, research on PEC aptasensors based on COFs remains in its infancy, motivating further development of COFs with both excellent photoactivity and high stability.

4. Modification strategies of photoactive materials

As the core component of PEC sensing, the photoelectric conversion efficiency of photoactive materials is closely related to the generation, migration, and redox capabilities of photogenerated charge carriers. Therefore, photoactive materials with high photoelectric conversion efficiency play a crucial role in improving the analytical performance of PEC biosensors. Although some single-component photoactive materials have been reported, they possess inherent limitations such as wide bandgaps, limited light absorption capacity, rapid recombination of photogenerated electron-hole pairs, and severe photo-corrosion. These drawbacks result in low photoelectric conversion efficiency, significantly impairing the analytical performance of PEC biosensing. Therefore, improving photon absorption as well as charge separation and transfer is essential to enhancing photoelectric conversion efficiency, which largely depends on the design of photoactive materials. This section introduces several strategies to improve the photoelectric conversion efficiency of photoactive materials in PEC aptasensors.

4.1. Morphology control

Rational regulation of the nanostructure of photoactive materials has emerged as a highly effective strategy for improving the performance of PEC aptasensors [123–125]. To date, various nanostructures have been synthesized and demonstrated photoelectrochemical properties, including one-dimensional (1D) nanotubes, nanobelts, nanowires, and nanorods, two-dimensional (2D) nanosheets and thin film, as well as three-dimensional (3D) microspheres, hollow microspheres, and nanoflowers [126–128]. In recent years, semiconductor nanocomposite photoactive materials based on 1D structures have been widely studied and applied in PEC aptasensors due to their excellent electron mobility at interface, high aspect ratio, and large specific surface area. For

example, Guo et al. utilized TiO_2/Sb_2S_3 nanorod arrays (NRAs) as key components of PEC biosensors for detecting miRNA-155 (an intracellular oncogenic miRNA) [129]. The cascade arrangement of energy levels, the dominant [hk1] direction of Sb_2S_3 NRAs, and the suitable bandgap of Sb_2S_3 enhanced charge separation and transport, as well as visible light harvesting. The carrier mobility of Sb_2S_3 NRAs has been reported to be approximately 10 $cm^2\ V^{-1}S^{-1}$, demonstrating efficient charge transfer along the nanorods. Similarly, Wei et al. prepared a ternary *Z*-scheme TiO_2-Ag-Ag_2S nanoarray (Fig. 4A) to effectively improve the transport pathways of photogenerated carriers while preserving the rod-shaped morphology of TiO_2, providing highly stable and accurate PEC performance [130]. Due to the high specific surface area, unique electronic and optical properties, and tunable band structure, 2D nanosheets have received widespread attention in PEC aptasensing platforms. The short diffusion pathways in 2D nanosheets accelerate exciton dissociation and free charge transfer. Meanwhile, the large surface area enables the absorption of a substantial number of photons in a remarkably short time, promoting the generation of more electron-hole pairs. Moreover, 2D nanosheets possess more active sites on their surface, providing significant advantages for probe attachment in PEC aptasensing. For example, Wang et al. synthesized $BiFeO_3$/ultrathin graphite-like carbon nitride (utg-C_3N_4) nanosheets [131]. Under visible light irradiation, the photocurrent of $BiFeO_3$/utg-C_3N_4 was 2.3 times that of $BiFeO_3$/bulk-C_3N_4. The large specific surface area of utg-C_3N_4 enabled the absorption of a large number of photons in a short time, and its ultrathin structure shortened the transport path of photogenerated charges, thereby improving PEC performance. In another study, Wang et al. successfully prepared Nd-MOF@AuNPs, where Nd-MOF nanosheets possessed a larger specific surface area, enabling higher AuNP loading and providing active sites for assembling sensing elements (Fig. 4B) [94]. Compared to solid materials, 3D hollow nanostructures impart unique characteristics to PEC processes. These include multiple light scattering generated by the hollow nanostructures, which enhances light-harvesting efficiency and absorption, as well as thin shells that reduce the charge carrier transmission distance, thereby improving charge separation (Fig. 4C) [132–135]. Bi et al. constructed a multimodal sensing platform based on 3D hollow CdS@Au nanospheres (HCdS@Au) for CEA detection, which combined PEC biosensors with colorimetric analysis and photothermal imaging [136]. The hollow CdS structure enhanced light absorption through scattering, resulting in higher photocurrents compared to solid SiO_2@CdS.

4.2. Doping/defect engineering

Doping refers to the introduction of impurities (metallic or non-metallic), known as "dopants" into a semiconductor material. This process effectively regulates the material's electronic structure and band position, thereby improving conductivity, narrowing the band gap, and

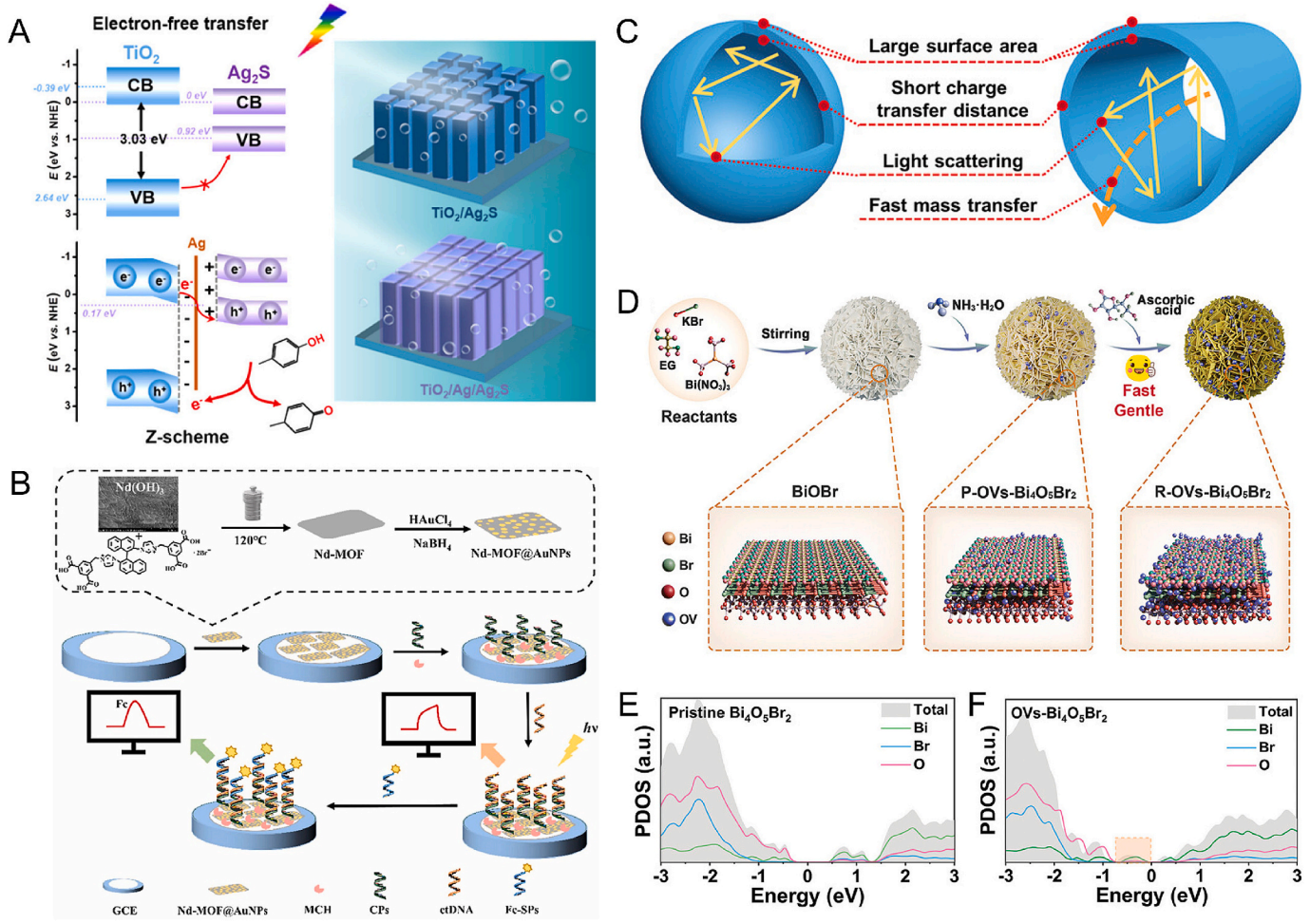

Fig. 4. (A) Schematic diagram of energy band diagram and charge separation path for TiO_2-Ag_2S and TiO_2-Ag-Ag_2S. (B) Schematic diagram of the preparation of Nd-MOF@AuNPs and the construction of PEC-EC dual-model circulating tumor DNA (ctDNA) biosensor. (C) Schematic diagram of some advantages of closed and open hollow structures. (D) Schematic diagram of the synthetic route of R-OVs-$Bi_4O_5Br_2$. (E) The calculated total and partial density of states of pristine $Bi_4O_5Br_2$ and (F) OVs-$Bi_4O_5Br_2$. Reprinted with permission Copyright 2022 American Chemical Society [130], Copyright 2023 Elsevier [94], and Copyright 2019 and 2024 Wiley [22,134].

enhancing carrier dynamics, which collectively improve PEC performance [137–139]. Currently, non-metallic elements such as N, P, B, S, and metallic elements such as Se, Zn, and Co have been explored as dopants for photoactive materials [140–142]. For example, Wei et al. developed a PEC biosensor using cysteine-induced BiOBr (cys-BiOBr) for the ultrasensitive detection of miRNA-155 [143]. Their research demonstrated that S doping *via* cysteine in BiOBr results in a 6-fold increase in photocurrent signal compared to undoped BiOBr. This indicates that S doping not only narrows the bandgap to enhance light absorption and accelerates carrier separation but also increases the surface oxygen vacancy concentration, which suppresses electron-hole pair recombination, thereby significantly improving photoelectric conversion efficiency. Liu et al. demonstrated that yttrium doping effectively addresses the limitations of insufficient light absorption and rapid carrier recombination in ZnO, thereby enhancing its photoelectric conversion efficiency [144]. Beyond to single-element doping, co-doping also exhibits great potential. For example, Wei et al. prepared Co/S co-doped BiOBr (Co/S-BiOBr) *via* a simple hydrothermal method [145]. The PEC signal of Co/S-BiOBr was twice that of S-BiOBr or Co-BiOBr alone and 12 times that of undoped BiOBr, which demonstrated that co-doping with Co and S reduced electron-hole pairs recombination and improved charge separation and transfer by modulating the electronic structure.

Compared to doping with foreign atoms, defect engineering is an effective strategy for tuning the electronic structure and improving PEC properties by introducing intrinsic defects into photoactive materials [146,147]. Defects can broaden the light absorption range by altering the band structure and introduce electronic states within the bandgap, thereby improving charge separation efficiency and carrier mobility [27]. However, in some cases, defect formation can reduce charge separation efficiency by creating recombination centers. Yin et al. prepared $Bi_4O_5Br_2$ with abundant oxygen vacancies (denoted as R-OVs-$Bi_4O_5Br_2$) (Fig. 4D) [22]. The introduction of oxygen vacancies (OVs) reduces the bandgap from 2.51 eV to 2.0 eV and extends the light absorption range from the original ~460 nm to ~540 nm. Theoretical calculations (Fig. 4E and F) indicate that the presence of OVs creates a new defect energy level in the bandgap of $Bi_4O_5Br_2$. These vacancies act as centers for capturing photogenerated electrons, greatly enhancing carrier separation efficiency and further improving PEC performance.

4.3. Heterojunction

In recent years, constructing heterojunctions has proven to be an effective method for improving the photoelectric conversion efficiency of photoactive materials. A heterojunction is an interface structure formed by aligning two or more semiconductor materials with different bandgap structures through band alignment. By employing appropriate band engineering, the light absorption range can be expanded, and the kinetics of charge transfer at the interface can be optimized, resulting in excellent performance in PEC aptasensors [148,149]. Based on the interfacial arrangement of the energy bands, heterojunctions can be classified into three types: straddling gap (type I), staggered gap (type II), and broken gap (type III) (Fig. 5A–5C) [150,151]. In type I heterojunction, the CB of one semiconductor (SC I) is higher than that of another semiconductor (SC II), while VB is lower than that of SC II. This band alignment causes photogenerated electrons and holes to transfer from SC I to SC II, resulting in enhanced carrier recombination. In type III heterojunction, the VB of SC I is lower than the CB of SC II, which prevents directional transport of photogenerated carriers between SC I and SC II. In type II heterojunction, both the CB and VB of SC I are higher than the corresponding bands of SC II. Photogenerated electrons in SC II transfer to SC I, while photogenerated holes in SC I transfer to SC II. This charge transfer pathway suppresses the rapid recombination of photogenerated electron-hole pairs and promotes their spatial separation. In recent decades, type II heterojunctions have been extensively utilized in photocatalysis and PEC due to their ability to facilitate effective charge separation and extend the lifetime of charge carriers through the classical mechanism of migration along the energy gradient and the creation of an internal electric field. For example, Feng et al. prepared hollow $CdIn_2S_4/In_2S_3$ heterostructure microspheres by a two-step hydrothermal

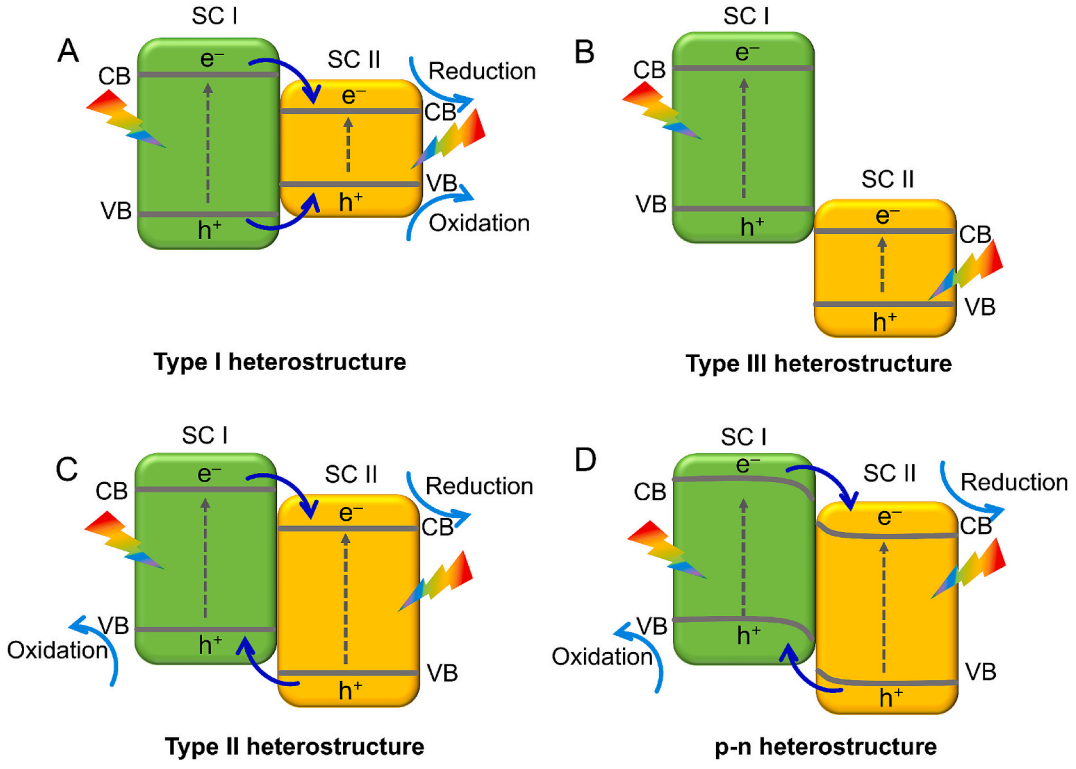

Fig. 5. The charge transfer mechanism of (A) Type-I heterojunction, (B) Type-III heterojunction, (C) Type-II heterojunction and (D) p-n heterojunction.

strategy [152]. The type II heterojunction formed by $CdIn_2S_4$ and In_2S_3 promotes charge separation, improved photoelectric conversion efficiency, and enhanced photocurrent response, thereby enabling accurate detection of hepatocellular carcinoma cells (HepG2 cells). Currently, numerous studies have focused on type II heterojunctions for constructing PEC aptasensors, including ZnO nanosheets/CdS QDs [153], $CuInS_2$/red phosphorus nanosheets [154], Ag:$ZnIn_2S_4/In_2O_3$ [155], poly(diphenylbutadiene)-BiOBr [156], polyvinylpyrrolidone-treated In_2S_3/WO_3 [157], WO_3/g-C_3N_4/Cu_2O-Au [158], Au@$BiVO_4/SnS_2$ [159], $MgTi_2O_5$/CdSe [160], CuO/BiOCl [161], $SnS_2/MgIn_2S_4$ [162], MoS_2/NbS_2 [163], BiOBr/Ag_2S [164], Bi_2S_3@BiOI/Ag_2S [165], b-TiO_2/CdS:Eu/Ti_3C_2 [166], Bi_2O_2S/Ag_2S [167], BiOI/TiO_2 [168]. In addition, p-n heterojunctions can be formed by combining p-type and n-type semiconductors. They typically exhibit built-in electric fields, which further promotes the transfer and separation of charge carriers (Fig. 5D) [131,169–171]. When p-type and n-type semiconductors come into contact, electrons from the n-type semiconductor diffuse into the p-type semiconductor, generating positive charges near the interface, while negative charges accumulate in the p-type semiconductor to balance the Fermi level (E_F). As a result, the region near the p-n interface becomes charged, forming an internal electric field. Under the influence of this internal electric field and upon light irradiation, photogenerated electrons and holes in the p-type and n-type semiconductors migrate to the CB of the n-type semiconductor and the VB of the p-type semiconductor, respectively. This leads to effective separation of electron-hole pairs and improves photoelectrochemical conversion performance. For example, Song et al. synthesized high-quality MoS_2 QDs-BiOI p-n heterojunction to construct a cathodic PEC aptasensing platform [172]. The photocurrent of the MoS_2 QDs-BiOI p-n heterojunction was nearly three times that of BiOI alone. Consequently, the proposed self-power cathodic PEC aptasensor achieved high sensitivity and accuracy in the determination of tumor necrosis factor-alpha (TNF-α, which is reported to relate to some cancers). Although type II heterojunctions effectively improve charge separation efficiency, the redox capability of photoexcited charge carriers is reduced compared to that of a single photoactive material. Unlike type II heterojunctions, photogenerated carriers in *Z*-scheme heterojunctions transport in a "Z" shape [173–175]. Specifically, under illumination, electrons in the CB of SC II can transfer to the holes in the VB of SC I, resulting in the accumulation of electrons in the more negative CB and holes in the more positive VB. Therefore, *Z*-scheme heterojunctions retain photogenerated electrons and holes with strong reduction and oxidation capabilities, facilitating efficient charge separation and enhanced redox activity. As early as 1979 [176], Bard proposed the ionic *Z*-scheme heterojunction (Fig. 6A), which required the use of appropriate redox pairs (*e.g.*, Fe^{3+}/Fe^{2+}, IO_3^-/I^-, and I_3^-/I^-) to facilitate charge transfer. However, due to the environmental limitations of ionic *Z*-scheme heterojunctions, Tada et al. introduced all-solid-state *Z*-scheme heterojunctions in 2006 (Fig. 6B) [177], employing a solid electronic conductor instead of redox pairs. Common solid electronic conductors include Au, Ag, Pt, Cu, Cd, W, and graphene oxide. For example, Tang et al. designed a PEC biosensor based on a *Z*-scheme heterojunction of TiO_2-Au-CdS QDs combined with CRISPR-Cas12a for detecting human papillomavirus-16 (HPV-16, the biomarker of cervical cancer and oropharyngeal cancer) (Fig. 6D) [178]. Wang et al. synthesized a ZnO/CdS heterojunction in 2009 and demonstrated that it followed the *Z*-scheme charge transfer mechanism when ZnO and CdS were in close contact [179]. In 2013, Yu et al. proposed the concept of direct *Z*-scheme heterojunction (Fig. 6C) [180]. Notably, direct Z-scheme heterojunctions inherited the advantages of traditional *Z*-scheme heterojunctions, including improved charge separation efficiency and optimized redox potential, without requiring solid electron conductors. So far, *Z*-scheme heterojunctions have been widely developed in PEC aptasensors. For example, our group synthesized a $Cu_2S/CdIn_2S_4$ direct Z-scheme heterojunction to achieve high PEC performance (Fig. 6E) [181]. Under illumination, the photocurrent of $Cu_2S/CdIn_2S_4$ was 6 times that of hollow Cu_2S, attributed to the strong internal electric field formed at the Z-scheme heterojunction, which promoted the separation and transfer of photogenerated carriers. Additionally, the hollow

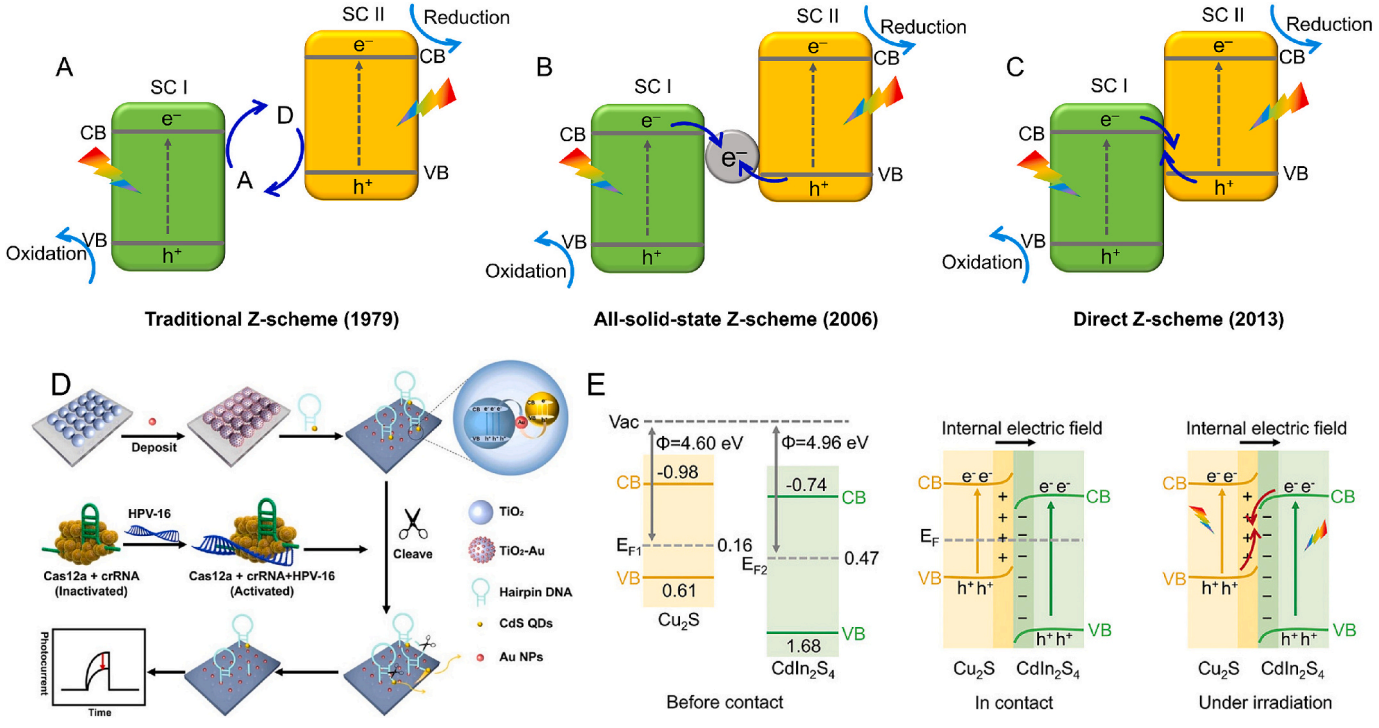

Fig. 6. The charge transfer mechanism of (A) traditional Z-scheme heterojunction, (B) all-solid-state Z-scheme heterojunction (C) direct *Z*-scheme heterojunction. (D) Schematic diagram of PEC biosensor based on TiO_2-Au-CdS QDs Z-scheme heterojunction for the detection of HPV-16. (E) Schematic diagram of charge transfer path of $Cu_2S/CdIn_2S_4$ before contact, in contact, and under irradiation. Reprinted with permission Copyright 2022 American Chemical Society [178] and Copyright 2024 Wiley [181].

structure of Cu_2S was beneficial for shortening the charge-transfer distance and improving light-harvesting ability.

To gain a deeper understanding of the direct Z-scheme charge transfer mechanism and thermodynamically questionable, Yu et al. introduced the concept of S-scheme heterojunctions in 2019 [182]. The S-scheme heterojunction revealed a charge transfer pathway resembling a "step" (macroscopic perspective) or an "N" (microscopic perspective) type, driven by enhanced built-in electric fields and band bending (Fig. 7A) [183–185]. This S-scheme heterojunction facilitated efficient charge separation and exhibits strong redox capabilities. Li et al. employed a SnO_2-OV/$CdIn_2S_4$ S-scheme heterojunction as a photoactive material to construct a PEC signal quenching sensor for the ultrasensitive detection of ctDNA (a biomarker of cancer) using multi-cycle strand displacement amplification combined with hybridization chain reaction (HCR) amplification (Fig. 7B) [186].

4.4. Schottky junction

The slow oxidation-reduction reaction at the photoelectrode/electrolyte interface can cause severe photocorrosion of semiconductors due to the accumulation of surface photogenerated charge carriers. Therefore, introducing efficient co-catalysts to promote interfacial redox reactions can issue this issue. The Schottky junction formed between a metal and a semiconductor provides catalytically active sites, thereby accelerating interfacial reaction kinetics and reducing charge recombination rates (Fig. 7C) [187–189]. When a metal contacts a semiconductor, electrons in the CB of semiconductor transfer toward the metal to equilibrate the E_F, thereby forming an electron depletion layer on the surface of the positive semiconductor and an electron accumulation layer in the negative metal region [4]. Therefore, the Schottky junction is beneficial for suppressing charge carrier recombination. Yan et al. constructed a biosensing platform with dual signal modes of colorimetry and PEC through a $Zn_{0.5}Cd_{0.5}S/Ti_3C_2$ (ZCS/TC) Schottky heterojunction [190], which was applied to monitor miRNA-21 (Fig. 7D). Density functional theory calculations demonstrated the formation of an intimate Schottky heterojunction between ZCS and TC, which facilitated charge separation and transfer, providing a satisfactory initial signal for subsequent implementation of PEC biosensors. Furthermore, LSPR of noble metal nanostructures (such as Ag and Au) generates high-energy hot electrons, promotes charge transfer in semiconductors, and enhances visible light absorption [191,192]. Fu et al. reported a CdS-NiS/Au composite material with high photoelectric conversion efficiency, exhibiting a photocurrent is 68 times higher than that of CdS alone, mainly due to the synergistic effect of the p-n heterojunction, Schottky junction, and the excellent optical properties of Au NPs [193]. By using Ag nanoclusters as effective quenchers combined with a duplex-specific nuclease (DSN) enzyme-assisted rolling circle amplification strategy, ultrasensitive detection of miRNA 21 with a LOD as low as 4.6 aM was achieved.

5. Sensing modes of PEC aptasensors

Tumor markers are substances associated with or produced by tumors and can be used for the early diagnosis of malignant tumors [38,194]. They provide a valuable and dynamic approach to understanding the full picture of cancer, and play an indispensable role in screening, diagnosis, and prognosis. Due to the superior affinity and specificity of aptamers for tumor markers, PEC aptasensors have shown great potential in tumor marker detection [195,196]. Based on the relationship between signal response and different target analyte concentrations, PEC aptasensors can be roughly divided into four modes: signal-off mode, signal-on mode, photocurrent polarity- switching

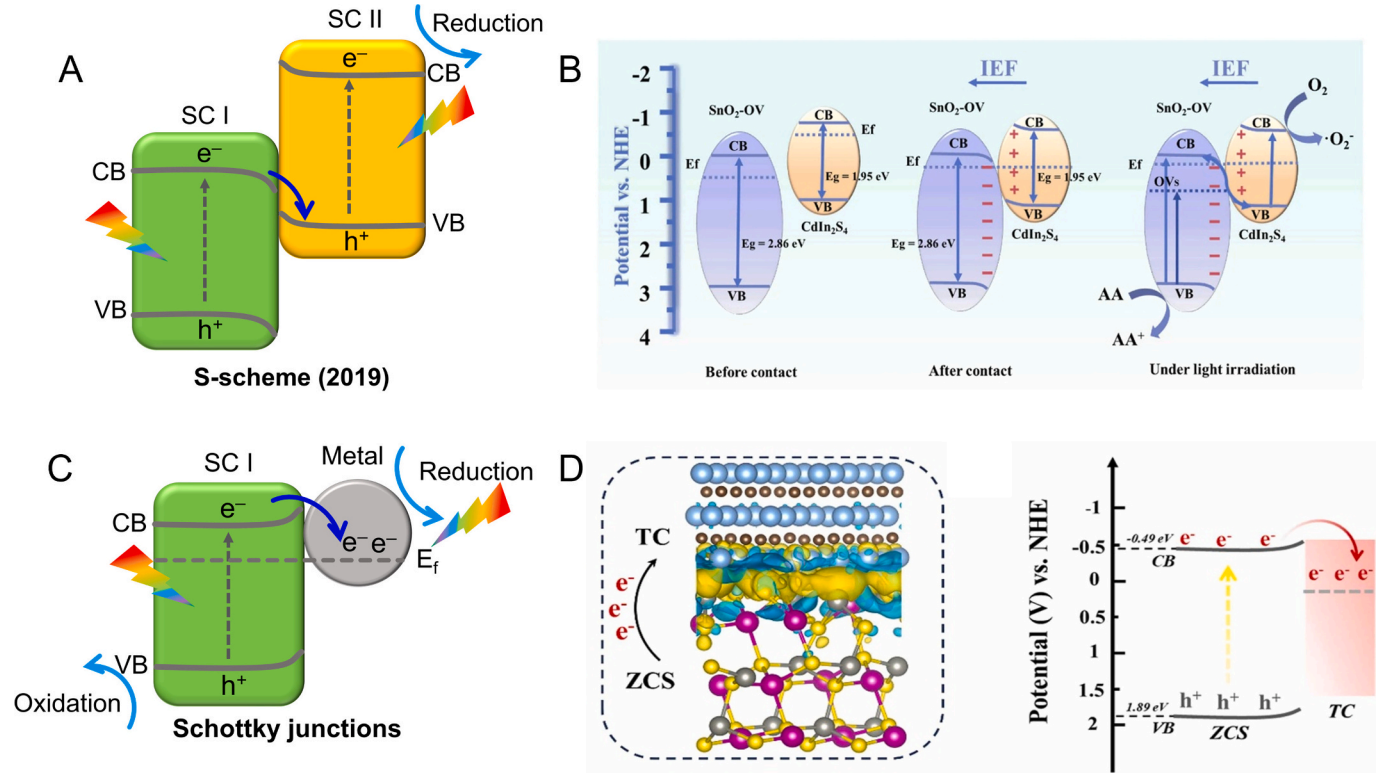

Fig. 7. The charge transfer mechanism of (A) S-scheme heterojunction. (B) Schematic diagram of charge transfer path of SnO_2-OV/$CdIn_2S_4$ before contact, after contact, and under irradiation. (C) The charge transfer mechanism of Schottky junction. (D) Differential charge density and possible mechanism of ZCS/TC. The depicted yellow and blue regions correspond to the accumulation and depletion of electrons, respectively. The yellow, gray, purple, blue, and brown spheres indicate S, Zn, Cd, Ti, and C atoms, respectively. Reprinted with permission Copyright 2025 and 2024 Elsevier [186,190]. (For interpretation of the references to colour in this figure legend, the reader is referred to the web version of this article.)

mode, and ratiometric mode. In this section, we summarize these four distinct modes of PEC aptasensors and discuss their signal amplification strategies for detecting tumor markers.

5.1. Signal-off mode

The PEC aptasensors based on signal-off mode typically exhibit a decrease in photocurrent with increasing target analyte concentration. Their analytical performance largely depends on a high initial photocurrent and effective signal quenching strategies. The initial photocurrent is achieved by utilizing photoactive materials with excellent PEC properties, as detailed in the preceding section on modification strategies of photoactive materials. Signal quenching strategies include the steric hindrance effect, p-n heterojunction quenching effect, and energy transfer (ET) effect [20,21,197]. The steric hindrance effect arises from the complex formed by the binding of the target analyte with an aptamer, which increases the steric hindrance on the electrode surface, thereby physically blocking charge transfer in the PEC aptasensor [198]. For example, Zhang et al. constructed a PEC aptasensor for detecting ATP based on Yb-doped Bi_2S_3 (Yb-Bi_2S_3) (Fig. 8A) [199]. In the presence of ATP, the steric hindrance effect arising from the formation of the ATP-aptamer complex increased steric hindrance at the electrode interface and hindered electron transfer, resulting in a significant decrease in photocurrent. In addition, enzyme-catalyzed precipitation reactions can serve as an effective method for quenching photocurrent by generating insoluble precipitates on the electrode surface, which suppresses interface electron transfer and significantly reduces the photocurrent signal [200]. Feng et al. developed a highly sensitive signal-off PEC aptasensor based on $Ag_2S/Ag/ZnIn_2S_4/C_3N_4$ for high-sensitivity detection of telomerase activity (TE, over-expression in most cancer cells) (Fig. 8B) [201]. In this system, Au NPs and Cu^{2+}-modified boron nitride nanosheets (AuNPs/Cu^{2+}-BNNS) acted as nanoenzymes to achieve significant amplification of PEC signals. The oxidation reaction between 4-chloro-1-naphthol and H_2O_2, catalyzed by nanoenzymes, generated insoluble precipitates on the electrode, hindering electron transfer and quenching the photocurrent. Besides, the p-n heterojunction quenching effect was achieved by utilizing p-type semiconductors to compete for photons and electron donors with n-type semiconductors, providing a simple and

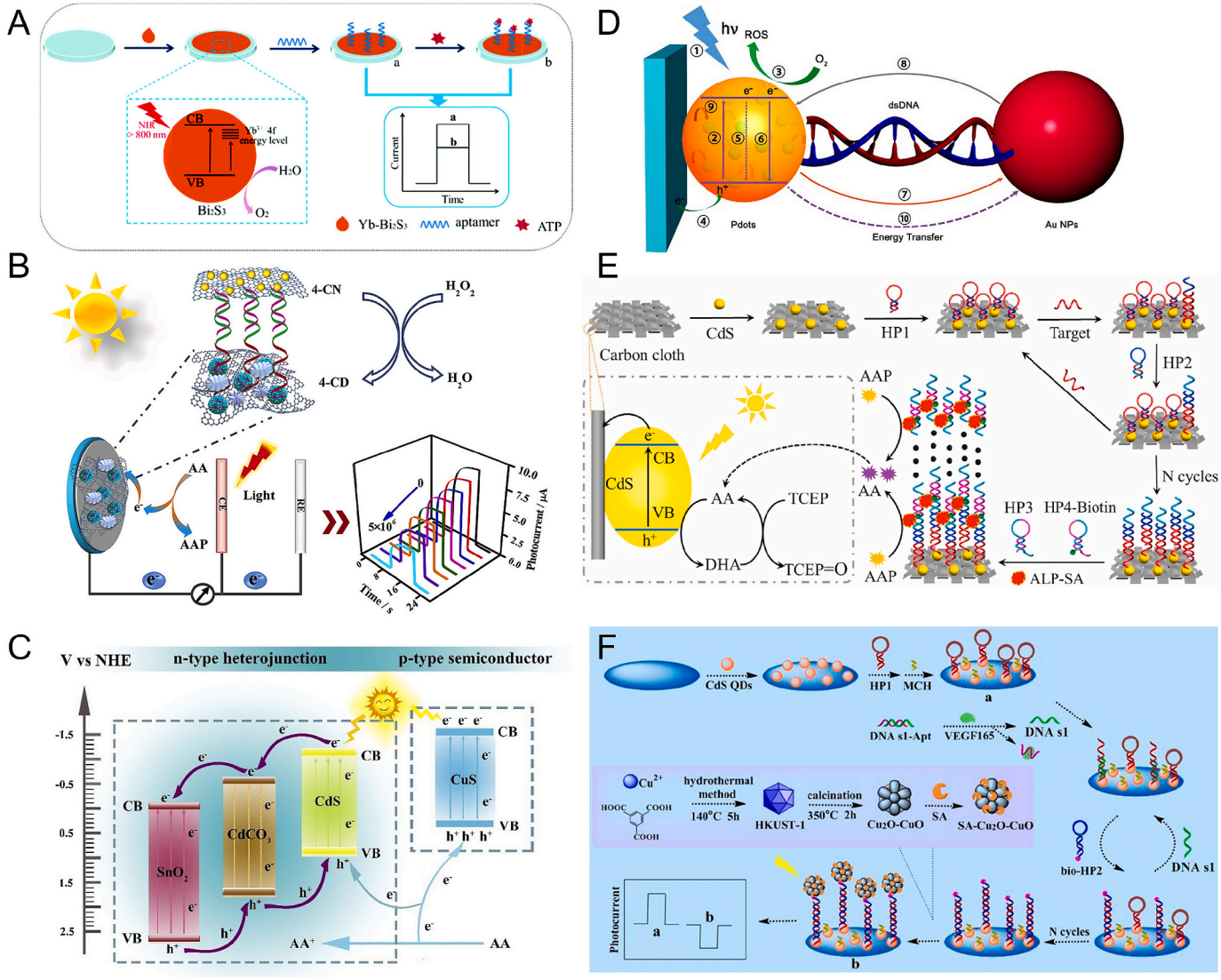

Fig. 8. (A) Schematic diagram of the signal-off PEC sensing platform for ATP detection by the steric hindrance effect. (B) Schematic diagram of the signal-off PEC aptasensor for TE activity detection by AuNPs/Cu^{2+}-BNNS nanozyme-mediated biocatalytic precipitation. (C) The photocurrent quenching mechanism of p-type CuS to n-type $SnO_2/CdCO_3/CdS$. (D) Schematic diagram of the PEC aptasensor based on ET between Pdots and Au NPs. (E) Schematic diagram of signal-on PEC biosensing by catalyzing the generation of AA. (F) Schematic diagram of the PEC sensing platform based on the porous Cu_2O-CuO flower-induced photocurrent-polarity switching of the CdS quantum dots. Reprinted with permission Copyright 2022 the Royal Society of Chemistry [199], Copyright 2022 and 2021 Elsevier [201,203,214], and Copyright 2018 and 2020 American Chemical Society [206,221].

effective method for constructing signal-off PEC biosensors [202]. Li et al. used n-type $SnO_2/CdCO_3/CdS$ with high photocurrent response as a signal indicator, and Y-type DNA structure stabilized p-type CuS QD was used as signal quencher to construct a p-n quenching PEC biosensor for detecting miRNA-21 (Fig. 8C) [203]. Upon the presence of miRNA-21, p-type CuS QD were introduced onto the electrode, significantly suppressing the photocurrent signal of $SnO_2/CdCO_3/CdS$. This was mainly attributed to the competition for electron donors and light energy between p-type CuS QD and n-type $SnO_2/CdCO_3/CdS$, as well as the steric effect of Y-type DNA structure. Luo et al. introduced many PbS QDs onto the electrode surface through catalytic hairpin assembly (CHA), significantly reducing the photocurrent of n-type $In_2O_3@Cu_2MoS_4$ and achieving quantitative detection of miRNA-21 [204]. Unlike steric hindrance and p-n heterojunction quenching effects, ET effect can regulate the behavior of photogenerated excitons by non-radiative energy coupling between donor and acceptor materials, thereby modulating the photocurrent signal. In 2011, Chen et al. first reported a strong ET effect between CdS QDs and AuNPs bridged by DNA biorecognition, and applied it to PEC biosensing [205]. In 2018, the same team reported the ET between polymer dots (Pdots) and Au NPs in a PEC aptasensor (Fig. 8D) [206]. When Au NPs approach Pdots, ET occurred, leading to a significant quenching of the photocurrent. It is worth noting that the quenching photocurrent induced by the ET effect must meet two conditions. First, the emission spectrum of the photoactive material must overlap with the absorption spectrum of the quenching nanomaterial to ensure efficient ET between the two. Second, a certain distance must be maintained between the two nanomaterials to enable ET to play a dominant role, thereby significantly reducing the photocurrent [207–209]. Furthermore, compared to single signal-off strategies, signal-off PEC aptasensors that integrate multiple quenching mechanisms can synergistically enhance sensitivity. For instance, Pan et al. proposed a PEC aptasensor for ultrasensitive detection of TNF-α based on the signal quenching effect of $NiCo_2O_4$-Au and the signal generator of H-CdS [210]. In the presence of TNF-α, $NiCo_2O_4$-Au is introduced onto the surface of the H-CdS electrode, resulting in competitive depletion of electron donors, p-n semiconductor quenching effect, and the mimetic enzymatic catalytic precipitation effect, leading to a significant decrease in photocurrent. Therefore, the PEC aptasensor can detect TNF-α at a lower LOD (0.63 fg mL^{-1}).

5.2. Signal-on mode

PEC aptasensors that exhibit a positive correlation between changes in photocurrent and the concentration of the identified target analyte belong to the "signal-on" mode. Compared to signal-off PEC aptasensors, signal-on PEC aptasensors are not limited by signal capacity [165]. Signal enhancement strategies in PEC aptasensing include *in situ* generation or release of electron donors/acceptors, sensitization effects, and LSPR effects [211–213]. Based on the strategy of *in situ* release of electron donors, Li et al. constructed a PEC biosensor for detecting miRNA-21. This sensor employed CdS NPs-modified carbon cloth as the photoactive material on polyimide films, combined with an efficient four-stage reaction system for target recognition and signal amplification (Fig. 8E) [214]. Specifically, the presence of miRNA-21 triggered the CHA and subsequent HCR, producing long dsDNA labeled with abundant alkaline phosphatase. This enzyme catalyzed the conversion of ascorbic acid 2-phosphate to AA. As an electron donor, AA was oxidized at the photoelectrode, initiating a redox cycling amplification process that regenerates AA and enhances the photocurrent response. Lei et al. developed a Y-shape-structured PEC biosensor for miRNA-222 (papillary thyroid carcinoma-relevant biomarker) detection based on a dual signal amplification strategy of Bi_4NbO_8Cl/TiO_2 heterojunction structure and *in situ* enzymatic generation of AA [215]. Sensitization effect refers to the combination of sensitizing materials (such as narrow bandgap semiconductors, conductive materials, and nanomaterials) with substrate materials to form an energy matched sensitizing structure. This improves the PEC performance and conductivity of the substrate, thereby enhancing detection sensitivity [216]. Fan et al. proposed a PEC biosensor for detecting miRNA-141 (a liver cancer marker) using AuNPs/$BiVO_4$ as photoactive materials, AgZnInS quantum dots as sensitizers, and a T7 Exo-assisted strand displacement dual recycle amplification reaction for signal amplification [217]. AgZnInS QDs formed a sensitized structure with $BiVO_4$, effectively separating photogenerated electron-hole pairs and significantly improving the photoelectric conversion efficiency. This resulted in a 5-fold increase in photocurrent response. Using a similar strategy, Mao et al. introduced the signal amplification factor H3-CdSe into a PEC biosensor based on the b-TiO_2/CdS:Eu/Ti_3C_2 heterojunction, achieving sensitive detection of miRNA-21 [166]. In addition to directly introducing sensitizing materials using labels, sensitizing structures can also be formed by *in situ* generation of photoactive substances. Lin et al. enhanced the photocurrent signal of Bi_2S_3@BiOI by *in situ* generating Ag_2S with a narrow bandgap, and constructed a split-type PEC biosensor for detecting CEA [165]. Furthermore, the LSPR effect enhanced light absorption and accelerated electron transfer, significantly increasing the photocurrent of photoactive materials. Lu et al. constructed a PEC biosensor for sensitive detection of MCF-7 cells (a type of human breast cancer cell) based on an organic PM6:Y6 p-n heterojunction [218]. The LSPR of Au NPs and Ag NPs generated by silver staining reaction enhanced the photocurrent response of the PEC biosensor and improved the sensitivity of the sensor with a LOD of 9 cell mL^{-1}. Wu et al. proposed a signal-on PEC biosensor for the sensitive detection of miRNA-155, which was based on DSN-assisted recycling amplification technology combined with photodeposited Ag enhanced $BiVO_4$ [219].

5.3. Photocurrent polarity-switching mode

Traditional PEC detection modes of signal-on and signal-off rely on changes in a single signal. However, in practical applications, the complexity of real samples often introduces multiple interfering substances, leading to false positive or false negative results [220]. Recently, innovative PEC strategies featuring unique photocurrent polarity-switching have been developed to overcome the limitations of traditional PEC analysis methods. A PEC aptasensor based on the photocurrent polarity-switching strategy generates a photocurrent signal with opposite polarity generate when the target analyte is present in the detection system [63]. This approach offers excellent selectivity and a low background signal. In 2019, Chen's group developed a PEC detection platform for VEGF165 assay (Fig. 8F) [221]. Through the VEGF165-induced CHA process, porous Cu_2O-CuO flowers were introduced onto CdS QDs, and the photocurrent polarity of CdS QDs was found to switch from anodic to cathodic, thereby improving the accuracy of PEC biosensors. To date, various nanomaterials have been applied in PEC aptasensors base on photocurrent polarity-switching strategies, such as ferrocene switching the photocurrent polarity of Cu doped ZnS NCs [222], p-type BiOBr switching the photocurrent polarity of n-type C_3N_5 [223], ZrO_2@CuO octahedra switching the photocurrent polarity of TiO_2 nanodisks [224], $CuBi_2O_4$ switching the photocurrent polarity of CdS QDs [225], G-wire switching the photocurrent polarity of In_2S_3 rods [226], $CuInS_2$ switching the photocurrent polarity of Er-MOF/AuNPs [95], and hemin/G-quadruplex switching the photocurrent polarity of $ZnIn_2S_4$ nanosheets [227], Au@Cu_2O switching the photocurrent polarity of CdS/Ni carbonate covalent organic framework nanorod arrays [228]. It should be noted that the success of the photocurrent polarity-switching strategy is not universally applicable but depends on the position of VB and CB of the photoactive materials, as well as appropriate band structure matching.

5.4. Ratiometric mode

The ratiometric PEC biosensor employs a dual-signal response mode, in which the ratio of two signals is used as the output signal rather than

the absolute value of a single signal [229]. The ratiometric PEC biosensors are usually divided into single-signal and dual-signal modes, depending on the target analyte. In single-signal mode, the target analyte causes a significant change in one signal, becoming the response signal, while the other signal remains relatively unchanged, becoming the reference signal. In dual-signal mode, the target analyte causes significant changes in both signals, which can serve as response or reference signals. Integrating ratio analysis technology into PEC aptasensors provides a built-in self-calibration model that effectively eliminates interference between the environment and detection system, thereby improving the sensitivity and accuracy of PEC analysis. So far, various ratiometric PEC aptasensors with wavelength, potential, and spatial-resolution have been successfully developed [230–232]. For example, Tang et al. constructed a ratiometric PEC aptasensor based on upconversion nanoparticles (UCNPs)-semiconductor nanocrystals (Fig. 9A) [233], using spatial-resolved technology, for detecting CEA. $NaYF_4$: Yb, Er UCNPs@CdTe nanocrystals were used as photoactive materials on two adjacent photoelectrodes, and CEA aptamer 1 (A1) and captured DNA (CA) covalently modified on both electrodes. Then, Au NP labeled CEA aptamer 2 (Au NP-A2) was immobilized on the functionalized

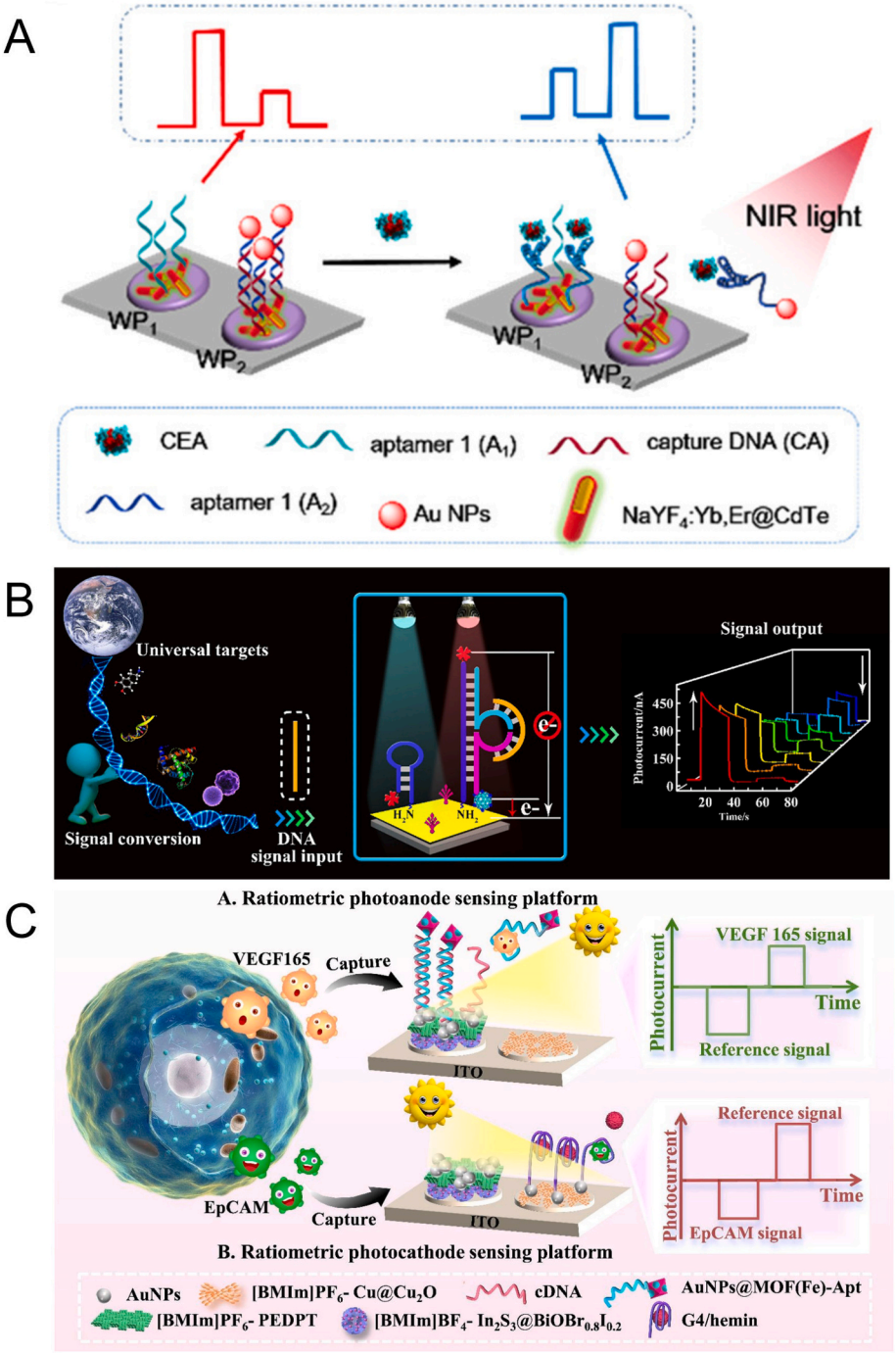

Fig. 9. (A) Schematic diagram of the upconversion-mediated ratiometric PEC aptasensor with spatial-resolved technique for CEA detection. (B) Schematic diagram of the ratiometric PEC bioassay with wavelength-resolved strategy for miRNA-141 detection. (C) Schematic diagram of the ratiometric PEC sensing platform with potential-resolved strategy for VEGF165 and EpCAM. Reprinted with permission Copyright 2019 and 2017 American Chemical Society [233,234], and Copyright 2024 Elsevier [235].

working photoelectrodes (WP2) surface to form dsDNA. After specific recognition of the target CEA, the photocurrent signal of WP1 weakened, while the photocurrent signal of WP2 significantly increased. Yuan et al. established a wavelength-resolved ratiometric PEC biosensor for detecting micRNA-141 by using two different photoactive materials (Fig. 9B) [234]. By utilizing target-nucleotide transduction-amplification technology and DNA nanomachine mediated electron-transfer tunnel distance regulation strategy, the photocurrent of SiO_2@MB near the sensing interface was enhanced at a wavelength of 623 nm, while the photocurrent of CdS QDs far from the sensing interface decreased at a wavelength of 460 nm. By calculating the ratio of these two different photocurrent signals, a ratiometric PEC analysis strategy was implemented. Zeng et al. proposed a dual-channel ratiometric PEC detection platform based on potential resolution for detecting VEGF165 and epithelial cell adhesion molecule (EpCAM, highly expressed in human epithelial cell-derived malignant tumors) (Fig. 9C) [235]. The platform immobilized ionic liquids sensitized In_2S_3@$BiOBr_{0.8}I_{0.2}$/polymerized 3,4-ethylenedioxythiophene/AuNPs (In_2S_3@$BiOBr_{0.8}I_{0.2}$/PEDOT/AuNPs) photoanode and Cu@Cu_2O photocathode on the same indium tin oxide electrode, with critical voltages of −0.13 V and 0.42 V, respectively. After assembling the adapted DNA in different potential response regions, the resulting PEC sensing platform enabled sensitive ratiometric PEC detection of VEGF165 and EpCAM by adjusting the threshold voltage.

6. Machine learning

In recent years, machine learning has demonstrated exceptional capabilities in processing complex datasets and extracting valuable information from large amounts of multidimensional detection data. It has become an efficient and indispensable tool across various applications in numerous research fields [236]. Significant advancements have been achieved in fields such as physics, chemistry, biology, and materials science by continuously iterating and modifying machine learning model data to improve efficiency and accuracy. In the field of biosensors, machine learning offers notable advantages, including the ability to extract meaningful analytical insights from noisy, low-resolution sensing data—such as signal amplitude, response time, and steady-state current—which often exhibit significant signal overlap [237,238]. Beyond noise reduction, machine learning techniques can predict outcomes from multivariate datasets by identifying inherent data patterns and extracting potential relationships from existing training data. This adaptability makes machine learning a powerful tool for addressing multivariate data challenges involving complex matrices or high-dimensional biological systems. Consequently, machine learning provides innovative solutions to overcome the limitations of multimodal biosensing systems [239]. Existing research has demonstrated the broad applicability and potential value of machine learning in designing effective catalysts and recognizing sensing signals. For example, Mohammadoor et al. employed machine learning to optimize the carbon dot synthesis process, thereby improving PEC performance [240]. Yang et al. combined PEC biosensors with machine learning to effectively distinguish cancer patients from healthy individuals, enhancing the sensitivity and accuracy of cancer diagnosis [241]. They also proposed a machine learning-assisted renewable and polarity-switchable PEC biosensor for intelligent diagnosis of circular RNA [242]. Their results showed the accuracy of about 100%, and acceptable sensitivity and specificity of circular RNA intelligent diagnosis. The integration of PEC sensors and machine learning holds great potential for the intelligent diagnosis of circular RNA-related cancers.

7. Conclusions and perspectives

Due to the high sensitivity, low background signal, and rapid response, PEC aptasensors have emerged as a highly promising method for the detection of tumor biomarkers. In particular, the rapid development of nanomaterials and nanotechnology has played a crucial role in advancing PEC aptasensors. To date, numerous semiconductor nanomaterials have been used to construct PEC aptasensors. Table 1 summarizes the detection performances of photoactive materials-based PEC aptasensors for tumor markers. Although PEC aptasensors have made significant progress, many challenges remain that hinder their widespread application and further development. To broaden their applications and enhance detection performance, the following development trends and challenges are presented:

(1) Although the development of photoactive materials plays a crucial role in promoting the widespread application of PEC aptasensors in various fields, issues such as high cost, insufficient stability, low photoelectric conversion efficiency, and complex synthesis cannot meet their large-scale commercial applications. Therefore, developing new photoactive materials with high photoelectric conversion efficiency, long-term stability, good biocompatibility, and advanced manufacturing processes remains an important issue. Perhaps machine learning can be used to accelerate the optimization and discovery of high-performance photoactive materials, uncovering underlying mechanisms and design principles, and providing new opportunities for the regulation and fabrication of functional photoactive materials.
(2) The utilization and regulation of photogenerated charge carriers often depend on assumptions or experimental conclusions. Although extensive research has been conducted, the fundamental mechanisms of photoelectrochemical reactions remain unclear, primarily due to the spatiotemporal complexity of charge separation, transfer, and participation in surface reactions. Advanced theoretical calculations and *in situ* characterization techniques (such as femtosecond transient absorption spectroscopy, Raman spectroscopy, Fourier infrared spectroscopy, *in situ* irradiated X-ray photoelectron spectroscopy, *etc.*) can provide a deeper understanding of the transport paths of charge carriers and the dynamic processes of charge separation and transfer. Surface reconstruction, identification of reaction sites, and photocorrosion phenomena also require the application of *in situ* electron microscopy or spectroscopy techniques to provide guidance for a deeper understanding of photoelectrochemical reaction mechanisms through complex theoretical calculations and characterization techniques.
(3) Most PEC sensing technologies typically use lamps as light sources, electrochemical workstations as signal conversion devices, and external power sources, which is inconsistent with the trend toward miniaturization and portability of detection devices. Therefore, future research should focus on developing high-performance portable PEC sensing devices. For example, integrating PEC sensing with microfluidics, arrays, and chips can achieve high throughput and automation. PEC sensing can also be combined with hand-held instruments and miniaturized signaling devices (smartphones, multimeters, pH meters, *etc.*) to achieve real-time detection. Moreover, most reported PEC sensors are still at the laboratory stage. Adopting interdisciplinary research methods can accelerate the commercialization of PEC sensing technology to meet the needs of practical applications. Integrating PEC sensing with other disciplines, with a focus on reliability, stability, and throughput.

CRediT authorship contribution statement

Si Zhang: Writing – original draft, Conceptualization. **Zihan Huang:** Validation. **Jiahui Sun:** Data curation. **Huangxian Ju:** Writing – review & editing, Conceptualization.

Table 1
Representative application of photoactive materials in PEC aptasensors for tumor marker detection.

Photoactive materials	Sensing mode	Target analyte	Detection range	LOD	Ref.
R-OVs-$Bi_4O_5Br_2$	Signal-on	MBD2	0.1–400 ng mL^{-1}	0.03 ng mL^{-1}	[22]
Br,N-codoped TiO_2	Signal-on	CEA	1 fg mL^{-1}–1 ng mL^{-1}	0.46 fg mL^{-1}	[50]
TiO_2/P5FIn	Signal-on Signal-off	GSH E2	0.5–1000 μM 367.1 fM–36.71 nM	167 nM 122.4 fM	[65]
$[(C6)_2Ir(dcbpy)]^+PF-$ 6/NiO	Signal-on	miRNA-122	0.1 fM–10 nM	36 aM	[72]
Bi-Bi_2O_3	Signal-off	miRNA-221	0.25 fM–2 nM	80 aM	[73]
AuNRs@end-TiO_2	Signal-on	miRNA-21	0.1 fM–100 pM	96 aM	[81]
SnS_2-GR	Signal-off	CEA	0.1 pg mL^{-1}–10 ng mL^{-1}	59.9 fg mL^{-1}	[85]
AuNPs/g-C_3N_4@TiO_2	Signal-on	5-mC	10 aM–0.1 μM	2.2 aM	[88]
NB-g-C_3N_4/CdS	Signal-off	miRNA-21	0.02–50 pM	1.1 fM	[89]
TBO@Bi_2S_3-ZnS	Signal-off	miRNA 21	10 aM–10 pM	3.3 aM	[102]
/	Polarity switching	CEA	10 fg mL^{-1}–1 ng mL^{-1}	3.98 fg mL^{-1}	[103]
ZrMOF	Polarity switching	VEGF165	0.01–500 pM	5.3 fM	[112]
$ZnIn_2S_4$@Zn-TCPP	Signal-off	miRNA-21	1 fM–1 nM	0.43 fM	[113]
dpMOF	Signal-on	VEGF165	1–1200 pM	0.43 pM	[114]
CdS NPs	Signal-on	CEA	1 fg mL^{-1}–10 ng mL^{-1}	0.36 fg mL^{-1}	[115]
$ZnIn_2S_4$	Signal-on	ATP	5 pM–10 nM	3.2 pM	[116]
AuNPs@WO_3@TpPa-1-COF	Signal-off	DNA methylation	10 fM–10 nM	0.19 fM	[121]
T-COF/Ag_2S	Signal-off	circSATB2	2 fM–500 pM	0.5 fM	[122]
TiO_2/Sb_2S_3 NRAs	Signal-on	miRNA-155	1 fM–0.1 μM	0.42 fM	[129]
TiO_2-Ag-Ag_2S	Signal-on	CD44	37–5 × 10^5 cells mL^{-1}	37 cells mL^{-1}	[130]
Nd-MOF@AuNPs	Signal-off	ctDNA	1 fM–10 nM	0.63 fM	[94]
HCdS@Au	Signal-off	CEA	0.015–2.4 ng mL^{-1}	3.5 pg mL^{-1}	[136]
cys-BiOBr	Signal-on	miRNA-155	0.5 fM–1 nM	0.13 fM	[143]
$CuInSe_2$/$Cu_3(BTC)_2$/Y:ZnO	Signal-on	miRNA-21	0.2 fM–2 nM	92 aM	[144]
Co/S-BiOBr	Signal-off	miRNA-221	1 fM–10 nM	0.24 fM	[145]
$CdIn_2S_4$/In_2S_3	Signal-off	HepG2 cells	100–2 × 10^5 cells mL^{-1}	23 cells mL^{-1}	[152]
Bi_2S_3@BiOI	Signal-on	CEA	0.005–50 ng mL^{-1}	1.21 pg mL^{-1}	[164]
b-TiO_2/CdS:Eu/Ti_3C_2	Signal-off	miRNA-21	1 μM–10 fM	3.3 fM	[166]
MoS_2 QDs-BiOI	Signal-off	TNF-α	10 fg mL^{-1}–0.1 μg mL^{-1}	5.2 fg mL^{-1}	[172]
TiO_2-Au	Signal-off	HPV-16	3 pM–600 nM	1 pM	[178]
Cu_2S/$CdIn_2S_4$	Signal-on	miRNA-141	0.1 fM–1 nM	32 aM	[181]
SnO_2-OV/$CdIn_2S_4$	Signal-off	ctDNA	0.1 fM–100 pM	21.8 aM	[186]
ZCS/TC	Signal-off	miRNAs-21	0.5 fM–1 nM	0.21 fM	[190]
CdS-NiS/Au	Signal-on	miRNA 21	10 aM–1 pM	4.6 aM	[193]
Yb-Bi_2S_3	Signal-off	ATP	0.5–300 nM	0.1 nM	[199]
Ag_2S/Ag/$ZnIn_2S_4$/C_3N_4	Signal-off	TE	50–5 × 10^5 cell mL^{-1}	19 cell mL^{-1}	[201]
SnO_2/$CdCO_3$/CdS	Signal-off	miRNA-21	10 fM–1 μM	3.25 fM	[203]
In_2O_3@Cu_2MoS_4	Signal-off	miRNA-21	1 fM–1 nM	0.57 fM	[204]
HCdS	Signal-off	TNF-α	1 fg mL^{-1}–1 ng mL^{-1}	0.63 fg mL^{-1}	[210]
CdS NPs	Signal-on	miRNA-21	1 fM–1 nM	0.41 fM	[214]
Bi_4NbO_8Cl/TiO_2	Signal-on	miRNA-222	1 pM–0.1 μM	0.15 pM	[215]
$BiVO_4$	Signal-on	miRNA-141	0.1 pM–10 nM	0.042 fM	[217]
PM6:Y6	Signal-on	MCF-7	10–1 × 10^4 cell mL^{-1}	9 cell mL^{-1}	[218]
$BiVO_4$	Signal-on	miRNA-155	10 aM–10 pM	8 aM	[219]
CdS QDs	Polarity switching	VEGF165	1–3000 fM	0.3 fM	[221]
$NaYF_4$:Yb,Er UCNPs@CdTe	Ratiometric	CEA	10 pg mL^{-1}–5 ng mL^{-1}	4.8 pg mL^{-1}	[233]
/	Ratiometric	miRNA-141	0.25 fM–25 pM	83.3 aM	[234]
[BMIm]BF_4-In_2S_3@$BiOBr_{0.8}I_{0.2}$/[BMIm]PF_6-PEDOT/AuNPs [BMIm]PF_6-Cu@Cu_2O	Ratiometric	VEGF165 EpCAM	10 fg mL^{-1}–0.5 μg mL^{-1} 10 pg mL^{-1}–0.1 μg mL^{-1}	2.03 fg mL^{-1} 996 fg mL^{-1}	[235]

Declaration of competing interest

The authors declare that they have no known competing financial interests or personal relationships that could have appeared to influence the work reported in this paper.

Acknowledgments

This work was financially supported by the National Natural Science Foundation of China (21827812, 21890741).

Data availability

Data will be made available on request.

References

[1] A.E. Becquerel, Recherches sur les effets de la radiation chimique de la lumiere solaire au moyen des courants electriques, Acad. Sci. 9 (1839) 145–149.
[2] A. Devadoss, P. Sudhagar, C. Terashima, K. Nakata, A. Fujishima, Photoelectrochemical biosensors: new insights into promising photoelectrodes and signal amplification strategies, J. Photochem. Photobiol. C 24 (2015) 43–63.
[3] S.T. Li, Y.H. Zhang, H.W. Huang, Black phosphorus-based heterostructures for photocatalysis and photoelectrochemical water splitting, J. Energy Chem. 67 (2022) 745–779.
[4] C.K. Xia, H. Wang, J.K. Kim, J.Y. Wang, Rational design of metal oxide-based heterostructure for efficient photocatalytic and photoelectrochemical systems, Adv. Funct. Mater. 31 (2021) 2008247.
[5] J. Shu, D.P. Tang, Recent advances in photoelectrochemical sensing: from engineered photoactive materials to sensing devices and detection modes, Anal. Chem. 92 (2020) 363–377.
[6] K. Song, H.J. Liu, B. Chen, C.C. Gong, J.W. Ding, T.F. Wang, E.Z. Liu, L.Y. Ma, N. Q. Zhao, F. He, Toward efficient utilization of photogenerated charge carriers in photoelectrochemical systems: engineering strategies from the atomic level to configuration, Chem. Rev. 124 (2024) 13660–13680.
[7] X.Y. Dong, W.H. Yang, L.Y. Hu, W.L. Gu, C.Z. Zhu, Recent advances in interface engineering for photoelectrochemical detection of new pollutants, Chem. Sci. 16 (2025) 18005–18022.
[8] Y.X. Dong, W.S. Wang, C.Q. Ye, Y.L. Song, Recent advances in photoelectrochemistry-coupled dual-modal biosensors: from constructions to biosensing applications, Nano Res. 17 (2024) 5512–5528.
[9] W.W. Zhao, J.J. Xu, H.Y. Chen, Photoelectrochemical DNA biosensors, Chem. Rev. 114 (2014) 7421–7441.

[10] W.W. Zhao, J.J. Xu, H.Y. Chen, Photoelectrochemical bioanalysis: the state of the art, Chem. Soc. Rev. 44 (2015) 729–741.
[11] G. Xiao, J.Z. Li, B.X. Zhao, Z. Yue, Photoelectrochemical aptasensors for biosensing: a review, Chemosensors 13 (2025) 344.
[12] Y.T. Xu, S.Y. Yu, Y.C. Zhu, G.C. Fan, D.M. Han, P. Qu, W.W. Zhao, Cathodic photoelectrochemical bioanalysis, Trends Anal. Chem. 114 (2019) 81–88.
[13] W.W. Tu, Z.Y. Wang, Z.H. Dai, Selective photoelectrochemical architectures for biosensing: design, mechanism and responsibility, Trends Anal. Chem. 105 (2018) 470–483.
[14] D.L. Hu, H.Y. Cui, X.Y. Wang, F. Luo, B. Qiu, W.C. Cai, H. Huang, J. Wang, Z. Y. Lin, Highly sensitive and selective photoelectrochemical aptasensors for cancer biomarkers based on MoS_2/au/GaN photoelectrodes, Anal. Chem. 93 (2021) 7341–7347.
[15] X. Tang, C.F. Lu, X.X. Xu, Z.H. Ding, H.Y. Li, H.J. Zhang, Y.Y. Wang, C.Y. Li, A visible and near-infrared light dual responsive "signal-off" and "signal-on" photoelectrochemical aptasensor for prostate-specific antigen, Biosens. Bioelectron. 202 (2022) 113905.
[16] X.K. Niu, M.M. Li, T.T. Liu, Y.D. Yang, J.T. Lu, X.M. Zhang, Three-dimensional DNA walker-mediated polarity switching biosensor based on the heterostructure of COFs and CuO nanocube for the sensitive photoelectrochemical detection of silver, Sens. Actuators B Chem. 426 (2025) 137019.
[17] A. Hanif, R. Farooq, M.U. Rehman, R. Khan, S. Majid, M.A. Ganaie, Aptamer based nanobiosensors: promising healthcare devices, Saudi Pharm. J. 27 (2019) 312–319.
[18] A.B. Iliuk, L.H. Hu, W.A. Tao, Aptamer in bioanalytical applications, Anal. Chem. 83 (2011) 4440–4452.
[19] X.X. Dong, A. Huang, L.L. He, C.Y. Cai, T.Y. You, Recent advances in foodborne pathogen detection using photoelectrochemical biosensors: from photoactive material to sensing strategy, Front. Sustain. Food Syst. 8 (2024) 14.
[20] Y.M. Fu, Q.H. Pan, Recent progress and challenges for improving the selectivity of photoelectrochemical biosensors, Microchem. J. 220 (2026) 116397.
[21] Y. Qin, J. Wen, X.S. Wang, L. Jiao, X.Q. Wei, H.J. Wang, J.L. Li, M.W. Liu, L. R. Zheng, L.Y. Hu, W.L. Gu, C.Z. Zhu, Iron single-atom catalysts boost photoelectrochemical detection by integrating interfacial oxygen reduction and enzyme-mimicking activity, ACS Nano 16 (2022) 2997–3007.
[22] L.L. Cao, Y.L. Zhou, L.L. Gao, H.S. Yin, M. Zhang, H.W. Zhang, P. Ju, K.P. Dou, S. Y. Ai, Ascorbic acid induced the improved oxygen vacancy defects of $Bi_4O_5Br_2$ and its application on photoelectrochemical detection of DNA demethylase MBD2 with improved detection sensitivity, Small 20 (2024) 2306365.
[23] L.B. Mao, Y. Xiao, H. Liu, X.H. Zhang, S.F. Wang, W.H. Huang, M.M. Chen, Water-stable $CsPbBr_3$/reduced graphene oxide nanoscrolls for high-performance photoelectrochemical sensing, Adv. Funct. Mater. 33 (2023) 2306365.
[24] C. Wang, X.Y. Song, Y. Wang, R. Xu, X.Y. Gao, C. Shang, P. Lei, Q.D. Zeng, Y. M. Zhou, B.L. Chen, P. Li, A solution-processable porphyrin-based hydrogen-bonded organic framework for photoelectrochemical sensing of carbon dioxide, Angew. Chem. Int. Ed. 62 (2023) e202311482.
[25] H.J. Zhao, T.T. Liu, F. Yang, Photoelectrochemical polarity-switching-mode and split-type biosensor based on SQ-COFs/BiOBr heterostructure for the detection of uracil-DNA glycosylase, Talanta 262 (2023) 124694.
[26] N.J. Li, C.Y. Wang, L.J. Chen, C. Ye, Y.W. Peng, Ultrathin covalent organic framework nanosheets/$Ti_3C_2T_x$-based photoelectrochemical biosensor for efficient detection of prostate-specific antigen, Molecules 27 (2022) 6732.
[27] J.F. Peng, L.J. Zu, Z.C. Ren, L. Liu, Z.Y. Yang, J.B. Chen, X.C. Wang, D.T. You, T. Guo, Synergistic integration of MoO_x co-catalyst with oxygen vacancies-engineered on $BiVO_4$ for enhancing the sensitivity of photoelectrochemical DNA biosensing, Chem. Eng. J. 477 (2023) 146989.
[28] H.T. Du, T.Y. Yin, J.R. Wang, G.F. Jie, Multifunctional photoelectrochemical biosensor based on $ZnIn_2S_4$/ZnS QDs@au–ag-reversed photocurrent of cu-metal-organic framework coupled with CRISPR/Cas-12a-shearing for assay of dual targets, Anal. Chem. 95 (2023) 7053–7061.
[29] J.Z. Cheng, B. Cheng, J.S. Xu, J.G. Yu, S.W. Cao, Organic-inorganic S-scheme heterojunction photocatalysts: design, synthesis, applications, and challenges, eScience 5 (2025) 100354.
[30] S. Mourdikoudis, S. Dutta, S. Kamal, S. Gómez-Graña, I. Pastoriza-Santos, S. Wuttke, L. Polavarapu, State-of-the-art, insights, and perspectives for MOFs-nanocomposites and MOF-derived (nano)materials, Adv. Mater. 37 (2025) 2415399.
[31] C. Zhang, M.Y. Wang, G.P. Li, L.N. Zou, Universal photoelectrochemical aptasensing platform for antibiotic based on $CuInS_2$/rGO and triplex DNA, Chem. Eng. J. 482 (2024) 149011.
[32] X. Chen, W.Q. Wu, Q. Zhang, C. Wang, Y.Y. Fan, H.M. Wu, Z.W. Zhang, Z-scheme Bi2O3/CuBi2O4 heterojunction enabled sensitive photoelectrochemical detection of aflatoxin b1 for health care, the environment, and food, Biosens. Bioelectron. 214 (2022) 114523.
[33] J. Yang, H.M. Zeng, Y.Q. Chai, R. Yuan, H.Y. Liu, Ultrasensitive photoelectrochemical biosensor amplified by target induced assembly of cruciform DNA nanostructure for the detection of dibutyl phthalate, Anal. Chim. Acta 1262 (2023) 341242.
[34] Y.X. Wen, S.G. Liu, B.X. Tao, H.Q. Luo, N.B. Li, A signal-off photocathode biosensor based on a novel metal-organic polymer for the detection of glucose, Sens. Actuators B 304 (2020) 127279.
[35] M.Q. Yang, L. Wang, H.Z. Lu, Y.C. Yang, S. Liu, Recent advances of functional nanomaterials for screen-printed photoelectrochemical biosensors, Acta Phys. -Chim. Sin. 41 (2025) 100018.
[36] Q. Liu, H. Zhang, H.H. Jiang, P.L. Yang, L.J. Luo, Q.J. Niu, T.Y. You, Photoactivities regulating of inorganic semiconductors and their applications in photoelectrochemical sensors for antibiotics analysis: a systematic review, Biosens. Bioelectron. 216 (2022) 114634.
[37] Z.G. Suo, T.F. Yu, Y.W. Xu, W.J. Ren, Y. Liu, M. Wei, H.L. Jin, B.S. He, R.Y. Zhao, Research progress of photoelectrochemical sensors in food detection, Food Res. Int. 206 (2025) 116071.
[38] J.J. Shi, Z.C. Chen, C.Q. Zhao, M.Q. Shen, H. Li, S.S. Zhang, Z. Zhang, Photoelectrochemical biosensing platforms for tumor marker detection, Coord. Chem. Rev. 469 (2022) 214675.
[39] K. Dashtian, F. Zahedpour, A. Foroozandeh, R. Karimi, M. Abdouss, S. Hajati, Recent trends in molecularly imprinted photoelectrochemical sensors, Trends Anal. Chem. 189 (2025) 118271.
[40] Y.L. Zhou, H.S. Yin, S.Y. Ai, Recent advances and applications of Bi_2S_3-based composites in photoelectrochemical sensors and biosensors, Trends Anal. Chem. 158 (2023) 116876.
[41] R. Rossetti, S. Nakahara, L.E. Brus, Quantum size effects in the redox potentials, resonance raman spectra, and electronic spectra of CdS crystallites in aqueous solution, J. Chem. Phys. 79 (1983) 1086–1088.
[42] L.E. Brus, A simple model for the ionization potential, electron affinity, and aqueous redox potentials of small semiconductor crystallites, J. Chem. Phys. 79 (1983) 5566–5571.
[43] J. Li, S.H. Liu, H. Dong, Y.Y. Li, Q. Liu, S.J. Wang, P. Wang, Y. Li, Y.Y. Li, Q. Wei, A ZnIn2S4/Ag2CO3 z-scheme heterostructure-based photoelectrochemical biosensor for neuron-specific enolase, Anal. Bioanal. Chem. 415 (2023) 5551–5562.
[44] M. Bruchez, M. Moronne, P. Gin, S. Weiss, A.P. Alivisatos, Semiconductor nanocrystals as fluorescent biological labels, Science 281 (1998) 2013–2016.
[45] W.C.W. Chan, S.M. Nie, Quantum dot bioconjugates for ultrasensitive nonisotopic detection, Science 281 (1998) 2016–2018.
[46] I. Willner, F. Patolsky, J. Wasserman, Photoelectrochemistry with controlled DNA-cross-linked CdS nanoparticle arrays, Angew. Chem. Int. Ed. 40 (2001) 1861–1864.
[47] J.J. Shan, Y. Cheng, M. Zhang, Y.H. Chang, B. Liu, Z. Li, Y.X. Song, D.J. Zang, Au-ag@ZnS quantum dots nanohybrid-enabled photoelectrochemical biosensing platform for highly sensitive detection of HPV 18 DNA, Electrochim. Acta 541 (2025) 147368.
[48] D.Y. Liao, G.F. Liang, Y.Y. Liu, W.J. Yan, Y.J. Guo, W.T. Liang, C. Dong, L.F. Fan, Design an efficient photoelectrochemical aptasensor for PCB72 based on CdTe@CdS core@shell quantum dots-decorated TiO_2 nanotubes, J. Hazard. Mater. 441 (2023) 129901.
[49] B.F. Xu, J. Zhang, A.P. Tanjung, F. Xu, A.J. Wang, L.P. Mei, P. Song, J.J. Feng, MOF-derived sandwich-structured dual Z-scheme Co_9S_8@$ZnIn_2S_4$/CdSe hollow nanocages heterojunction: target-induced ultrasensitive photoelectrochemical sensing of chlorpyrifos, Biosens. Bioelectron. 257 (2024) 116324.
[50] Y.H. Zhang, M.J. Li, H.J. Wang, R. Yuan, S.P. Wei, Supersensitive photoelectrochemical aptasensor based on Br,N-codoped TiO_2 sensitized by quantum dots, Anal. Chem. 91 (2019) 10864–10869.
[51] K. Song, J.W. Lin, Y.F. Zhuang, Z.Z. Han, J.H. Chen, Construction of photoelectrochemical DNA biosensors based on TiO_2@carbon dots@black phosphorous quantum dots, Micromachines 12 (2021) 1523.
[52] D. Gholamin, P. Karami, Y. Pahlavan, M. Johari-Ahar, Highly sensitive photoelectrochemical immunosensor for detecting cancer marker CA19-9 based on a new SnSe quantum dot, Microchim. Acta 190 (2023) 154.
[53] M.J. Xiao, M.H. Zhu, R. Yuan, Y.L. Yuan, Dual-sensitized heterojunction PDA/ZnO@MoS_2 QDs combined with multilocus domino-like DNA cascade reaction for ultrasensitive photoelectrochemical biosensor, Biosens. Bioelectron. 227 (2023) 115151.
[54] M.S. Hu, J.J. Wang, J.X. Han, Y.M. Rong, H.H. Yu, S.G. Ge, H.M. Yang, L. N. Zhang, J.H. Yu, Nuclease-propelled target dual-recycling amplification strategy integrated with cascaded sensitization effect of ZnO/$CuInS_2$/Ag_2Se photoactive structures for lab-on-paper photoelectrochemical miRNA bioassay, Sens. Actuators B 369 (2022) 132374.
[55] H.C. Geng, X.X. Chen, L.L. Sun, Y. Qiao, J. Song, S.S. Shi, Q.Y. Cai, ZnCuInSe/au/TiO_2 sandwich nanowires-based photoelectrochemical biosensor for ultrasensitive detection of kanamycin, Anal. Chim. Acta 1146 (2021) 166–173.
[56] C.X. Li, S.J. Wang, L.F. Zhu, K.Y. Liu, L.Y. Jing, L. Xie, S.G. Ge, J.H. Yu, $Cs_3Bi_2Br_9$ QDs/BiOBr heterojunction photoelectrochemical biosensor with APE1 enzyme-driven bipedal DNA walker signal amplification for miRNA-320d detection, Anal. Chim. Acta 1379 (2025) 344713.
[57] Q.Q. Cai, H.K. Li, W.S. Dong, G.F. Jie, Versatile photoelectrochemical biosensor based on AIS/ZnS QDs sensitized-WSe_2 nanoflowers coupled with DNA nanostructure probe for "on-off" assays of TNF-α and MTase, Biosens. Bioelectron. 241 (2023) 115704.
[58] S.P. Wang, F.F. Wang, C.P. Fu, Y.N. Sun, J.G. Zhao, N. Li, Y.Q. Liu, S.G. Ge, J. H. Yu, $AgInSe_2$-sensitized ZnO nanoflower wide-spectrum response photoelectrochemical/visual sensing platform via au@Nanorod-anchored CeO_2 octahedron regulated signal, Anal. Chem. 92 (2020) 7604–7611.
[59] N.S. Hassan, A.A. Jalil, N.F. Khusnun, A. Ahmad, T.A.T. Abdullah, R.M. Kasmani, N. Norazahar, M.F.A. Kamaroddin, D.V.N. Vo, Photoelectrochemical water splitting using post-transition metal oxides for hydrogen production: a review, Environ. Chem. Lett. 20 (2022) 311–333.
[60] Y.Z. Chen, D.J. Jiang, Z.Q. Gong, J.Y. Li, L.N. Wang, Anodized metal oxide nanostructures for photoelectrochemical water splitting, Int. J. Miner. Metall. Mater. 27 (2020) 584–601.
[61] A. Fujishima, K. Honda, Electrochemical photolysis of water at a semiconductor electrode, Nature 238 (1972) 37–38.

[62] W. Lu, G. Wang, Y. Jin, X. Yao, J.Q. Hu, J.H. Li, Label-free photoelectrochemical strategy for hairpin DNA a hybridization detection on titanium dioxide electrode, Appl. Phys. Lett. 89 (2006) 263902.

[63] W.C. Geng, G.H. Jiang, H.M. Liu, L.S. Xue, L.H. Ding, Y.L. Li, Y.J. Wu, R.Y. Yang, A direct-contact photocurrent-direction-switching biosensing platform based on in situ formation of CN QDs/TiO_2 nanodiscs and double-supported 3D DNA walking amplification, Small 19 (2023) 2302829.

[64] R. Hu, X.X. Ren, P. Song, A.J. Wang, L.P. Mei, J.J. Feng, Hollow cage-like PtCu nanozyme-regulated photo-activity of porous $CdIn_2S_4/SnO_2$ heterojunctions for ultrasensitive PEC sensing of streptomycin, Biosens. Bioelectron. 236 (2023) 115425.

[65] L. Zhang, D.D. Liu, A.Z. Wang, J.D. Zhang, X.Y. Yang, G.M. Nie, Photoelectrochemical biosensor based on TiO2/P5FIn with a cascade amplification strategy for simultaneous detection of GSH and e2 analytes of ovarian cancer, Anal. Chem. 97 (2025) 6594–6599.

[66] G.L. Wang, J.J. Xu, H.Y. Chen, S.Z. Fu, Label-free photoelectrochemical immunoassay for α-fetoprotein detection based on TiO_2/CdS hybrid, Biosens. Bioelectron. 25 (2009) 791–796.

[67] C.Z. Zhong, C.Z. Zhang, Y. Yang, X.X. Liang, Q. Pang, L.Y. Zhou, P.C. Chen, Synergistic effect of photoelectrochemical aptasensor based on staggered gap ZnO/$BiFeO_3$ heterojunction coupled with cDNA-CdS sensitizer enabling ultrasensitive assay of kanamycin, Food Chem. 437 (2024) 137877.

[68] J.J. Yao, X.H. Feng, S.Q. Wang, Y.M. Liang, B.T. Zhang, Plasmon-enhanced photoelectrochemistry of photosystem II on a hierarchical tin oxide electrode for ultrasensitive detection of 17β-estradiol, Anal. Chem. 96 (2024) 18029–18036.

[69] S. Zhang, H.J. Zheng, R.J. Jiang, J.F. Yuan, F. Li, T.T. Qin, A. Sakthivel, X.Q. Liu, S. Alwarappan, Ultrasensitive PEC aptasensor based on one dimensional hierarchical SnS_2|oxygen vacancy-WO_3 co-sensitized by formation of a cascade structure for signal amplification, Sens. Actuators B 351 (2022) 130966.

[70] Y. Zhao, W. Li, Z.L. Song, G.C. Fan, X.L. Luo, Integrating bifunctional peptide on a cu-MOF/Cu2O photocathode: toward an anti-interference and sensitive photoelectrochemical protein biosensor, Anal. Chem. 97 (2025) 14700–14708.

[71] W.X. Dai, L. Zhang, W.W. Zhao, X.D. Yu, J.J. Xu, H.Y. Chen, Hybrid PbS quantum dot/nanoporous NiO film nanostructure: preparation, characterization, and application for a self-powered cathodic photoelectrochemical biosensor, Anal. Chem. 89 (2017) 8070–8078.

[72] M.W. Lv, C.X. Zong, X.D. Chen, X.J. Lin, L.H. Kong, C.X. Li, A cathodic photoelectrochemical biosensor based on CRISPR/Cas12a trans-cleavage mediated p-n heterojunction quenching mode for microRNA determination, Anal. Chim. Acta 1268 (2023) 341399.

[73] H.H. Yu, C.Y. Tu, H.S. Liu, L.N. Zhang, C.M. Gao, Y. Zhang, P.H. Zhu, S.G. Ge, H. M. Yang, J.H. Yu, Hot-hole injection-enabled efficient signal modulation for boosting sensitive paper-based photocathodic analysis through an atom-shared plasmonic hetero-nanostructure, Anal. Chem. 97 (2025) 8528–8536.

[74] F. Mo, W. Li, J.J. Zhao, Y. Zheng, Q. Sun, X.Z. Huang, G.Q. Wu, Y.J. Zhang, Y. F. Shen, Recent advances in photoelectroanalysis: carbon-containing materials for enhanced sensing performance, Adv. Funct. Mater. 35 (2025) 2504679.

[75] Y.J. Chung, J. Kim, C.B. Park, Photonic carbon dots as an emerging nanoagent for biomedical and healthcare applications, ACS Nano 14 (2020) 6470–6497.

[76] H.Y. Zhang, W.J. Tian, X.G. Duan, H.Q. Sun, Y.L. Shen, G.S. Shao, S.B. Wang, Functional carbon nitride materials for water oxidation: from heteroatom doping to interface engineering, Nanoscale 12 (2020) 6937–6952.

[77] Q.W. Huang, X.L. Lin, D.X. Nie, J. Wang, K. Fan, Z.Z. Zhao, Z. Han, Enhanced electrochemical and photochemical sensors for in vivo biological monitoring based on carbon nanomaterials, Adv. Funct. Mater. 35 (2025) 2503027.

[78] R. Yuan, B.D. Yan, C.Y. Lai, X.H. Wang, Y. Cao, J.C. Tu, Y. Li, Q. Wu, Carbon dot-modified branched TiO_2 photoelectrochemical glucose sensors with visible light response, ACS Omega 8 (2023) 22099–22107.

[79] Y.H. Zhu, Z.W. Xu, J. Gao, W.H. Ji, J.D. Zhang, An antibody-aptamer sandwich cathodic photoelectrochemical biosensor for the detection of progesterone, Biosens. Bioelectron. 160 (2020) 112210.

[80] H.X. Zhao, H.Y. Qi, T.H. Yi, T. Jing, J. Li, S.Q. Shen, Q.X. Zeng, Y. Gao, Quantum yield of carbon dots adjusts the performance of TiO_2-In_2S_3-based photoelectrochemical biosensor for alpha-fetoprotein detection, Microchem. J. 212 (2025) 113115.

[81] J. Yang, W.X. Li, L.H. Guo, F. Luo, B. Qiu, Z.Y. Lin, L.X. Wang, Highly sensitive photoelectrochemical biosensor for microRNA-21 based on a dumbbell-shaped heterostructure AuNRs@end-TiO_2 combined with carbon dots as photosensitizers and duplex-specific nuclease-assisted signal amplification, Anal. Chem. 94 (2022) 13575–13581.

[82] Q.Z. Han, H.Y. Wang, D. Wu, Q. Wei, Preparation of PbS NPs/RGO/NiO nanosheet arrays heterostructure: function-switchable self-powered photoelectrochemical biosensor for H2O2 and glucose monitoring, Biosens. Bioelectron. 173 (2021) 112803.

[83] K.S. Novoselov, A.K. Geim, S.V. Morozov, D. Jiang, Y. Zhang, S.V. Dubonos, I. V. Grigorieva, A.A. Firsov, Electric field effect in atomically thin carbon films, Science 306 (2004) 666–669.

[84] X. Huang, Z.Y. Yin, S.X. Wu, X.Y. Qi, Q.Y. He, Q.C. Zhang, Q.Y. Yan, F. Boey, H. Zhang, Graphene-based materials: synthesis, characterization, properties, and applications, Small 7 (2011) 1876–1902.

[85] D. Huang, L. Wang, Y. Zhan, L.N. Zou, B.X. Ye, Photoelectrochemical biosensor for CEA detection based on SnS_2-GR with multiple quenching effects of au@CuS-GR, Biosens. Bioelectron. 140 (2019) 111358.

[86] M.J. Li, Y. Wu, S.Y. An, Z.T. Yan, Au NP-decorated g-C_3N_4-based photoelectochemical biosensor for sensitive mercury ions analysis, ACS Omega 7 (2022) 19622–19630.

[87] S.S. Low, Z. Chen, Y.R. Li, Y.L. Lu, Q.J. Liu, Design principle in biosensing: critical analysis based on graphitic carbon nitride (G-C3N4) photoelectrochemical biosensor, Trends Anal. Chem. 145 (2021) 116454.

[88] C.Y. Zhu, X. Tian, Q.Y. Li, Z.C. Dai, L.N. Wang, H.M. Liu, C.H. Li, K.R. Zahid, C. M. Wu, H. Huang, L.C. Fang, Q.Y. Huang, F.X. Liu, J. Deng, Y. Li, T. Zeng, J. S. Zheng, Ultrasensitive photoelectrochemical biosensor for DNA 5-methylcytosine analysis based on co-sensitization strategy combined with bridged DNA nanoprobe, Talanta 254 (2023) 124140.

[89] Q.Y. Du, H.Y. Zhang, Y.N. Bi, H.J. Wang, X.M. Zhou, P.F. Shi, S.Z. Lv, S. Bi, N-deficient b-doped g-C3N4/CdS heterojunction-based PEC-FL biosensor assisted by CRISPR-Cas12a system for ultrasensitive determination of microRNA, Anal. Chem. 97 (2025) 4049–4056.

[90] W. Wu, Y. Hong, Y. Zhou, Q. Sun, J. Huang, Y. Wang, C. Li, D. Sun, A photocurrent polarity switching photoelectrochemical aptasensor based on Er-MOF nanosheets and methylene blue for high-performance determination of CA15-3, Anal. Chim. Acta 1404 (2026) 345454.

[91] Y. Li, W. Cai, M. Xu, M. Wang, L. He, C. Guo, M. Wang, Z. Zhang, N. Zhou, Construction of a near-infrared light-assisted two-electrode self-powered photoelectrochemical aptasensor for sensitively aptasensing carbohydrate antigen and colorectal cancer CT26 cells, Microchem. J. 195 (2023) 109449.

[92] K. Song, Y. Roh, H. Park, J.Y. Park, Plasmonic hot carrier-driven photoelectrochemical processes: principle, detection and application, Adv. Mater. Interfaces 12 (2025) 2400273.

[93] M. Valenti, M.P. Jonsson, G. Biskos, A. Schmidt-Ott, W.A. Smith, Plasmonic nanoparticle-semiconductor composites for efficient solar water splitting, J. Mater. Chem. A 4 (2016) 17891.

[94] R.Y. Zha, R.Y. Wu, Y.G. Zong, Z.G. Wang, T. Wu, Y.Y. Zhong, H.P. Liang, L. F. Chen, C.Y. Li, Y.Y. Wang, A high performance dual-mode biosensor based on Nd-MOF nanosheets functionalized with ionic liquid and gold nanoparticles for sensing of ctDNA, Talanta 258 (2023) 124377.

[95] Y.W. Hong, H.W. Sun, W. Wu, Q.F. Lin, X.Y. Chen, Y.Y. Wang, D. Sun, C.Y. Li, J. M. Qu, A photocurrent polarity switching photoelectrochemical aptasensor based on Er-MOF nanocubes and $CuInS_2$ nanoflowers for the efficient determination of miRNA-21, Sens. Actuators B 450 (2026) 139202.

[96] Y. Zhong, X. Wang, R. Zha, C. Wang, H. Zhang, Y. Wang, C. Li, Dual-wavelength responsive photoelectrochemical aptasensor based on ionic liquid functionalized Zn-MOFs and noble metal nanoparticles for the simultaneous detection of multiple tumor markers, Nanoscale 13 (2021) 19066.

[97] L. Cui, J.Z. Shen, C.C. Li, P.P. Cui, X.L. Luo, X.L. Wang, C.Y. Zhang, Construction of a dye-sensitized and gold plasmon-enhanced cathodic photoelectrochemical biosensor for methyltransferase activity assay, Anal. Chem. 93 (2021) 10310–10316.

[98] H.R. Cheng, Y.F. Wang, Y.R. Zhao, H.M. Hou, G.L. Zhang, J.R. Bi, S. Yan, H. S. Hao, Hybrid chain reaction-based and au/Bi4NbO8Cl/In2S3 layer-by-layer assembled dual-mode photoelectrochemical-electrochemical aptasensor for the detection of salmonella enteritidis, Talanta 281 (2025) 126815.

[99] H.J. Dai, W. Ahmad, S.M. Zhang, L. Wang, K.X. Zou, X.Y. Lin, J. Wei, M. Chen, Q. S. Chen, A.H. Lin, X.M. Chen, A visible-light-driven self-powered nodularin-R biosensing platform controlled by an integrated portable photoelectrochemical detection device, Anal. Chem. 96 (2024) 12526–12534.

[100] Z.Y. Yan, Z.H. Wang, Z. Miao, Y. Liu, Dye-sensitized and localized surface plasmon resonance enhanced visible-light photoelectrochemical biosensors for highly sensitive analysis of protein kinase activity, Anal. Chem. 88 (2016) 922–929.

[101] X.Y. Yang, M.J. Zhang, Z.X. Chen, Y.W. Bu, X. Gao, Y.K. Sui, Y.Q. Yu, Sodium alginate micelle-encapsulating zinc phthalocyanine dye-sensitized photoelectrochemical biosensor with CdS as the photoelectric material for hg2+ detection, ACS Appl. Mater. Interfaces 13 (2021) 16828–16836.

[102] H. Meng, P.K. Liu, F.J. Mo, M. Chen, Y.Z. Fu, A novel ultrasensitive photoelectrochemical biosensor for detecting microRNA 21 based on cosensitization strategy and p-n heterojunction quenching mode, Sens. Actuators B 325 (2020) 128782.

[103] F. Mo, M. Han, X. Weng, Y.Y. Zhang, J. Li, H.B. Li, Magnetic-assisted methylene blue-intercalated amplified dsDNA for polarity-switching-mode photoelectrochemical aptasensing, Anal. Chem. 93 (2021) 1764–1770.

[104] M.Z. Lv, W. Zhou, H. Tavakoli, C. Bautista, J.F. Xia, Z.H. Wang, X.J. Li, Aptamer-functionalized metal-organic frameworks (MOFs) for biosensing, Biosens. Bioelectron. 176 (2021) 112947.

[105] L. Gorgani, M. Mohammadi, G. Najafpour Darzi, J.B. Raoof, Metal-organic framework (MOF)-based biosensors for miRNA detection, Talanta 273 (2024) 125854.

[106] O.M. Yaghi, G.M. Li, Hailian li, Selective binding and removal of guests in a microporous metal-organic framework, Nature 378 (1995) 703–706.

[107] J.P. Lei, R.C. Qian, P.H. Ling, L. Cui, H.X. Ju, Design and sensing applications of metal-organic framework composites, Trends Anal. Chem. 58 (2014) 71–78.

[108] J. Haider, A. Shahzadi, M.U. Akbar, I. Hafeez, I. Shahzadi, A. Khalid, A. Ashfaq, S. O.A. Ahmad, S. Dilpazir, M. Imran, M. Ikram, G. Ali, M. Khan, Q. Khan, M. Maqbool, A review of synthesis, fabrication, and emerging biomedical applications of metal-organic frameworks, Biomater. Adv. 140 (2022) 213049.

[109] W.S. Kong, D. Zhu, R.G. Luo, S.Q. Yu, H.X. Ju, Framework-promoted charge transfer for highly selective photoelectrochemical biosensing of dopamine, Biosens. Bioelectron. 211 (2022) 114369.

[110] W.P. Jiang, Z.J. Li, Q.L. Yang, X.D. Hou, Integration of metallic nanomaterials and recognition elements for the specifically monitoring of pesticides in electrochemical sensing, Crit. Rev. Anal. Chem. 54 (2024) 2636–2657.

[111] C.T. Hou, J.Y. Peng, Q. Xu, Z.P. Ji, X.Y. Hu, Elaborate fabrication of MOF-5 thin films on a glassy carbon electrode (GCE) for photoelectrochemical sensors, RSC Adv. 2 (2012) 12696–12698.
[112] W.S. Kong, Z.Y. Xu, T.R. Liu, J.P. Lei, H.X. Ju, Photocurrent polarity reversal induced by electron-donor release for the highly sensitive photoelectrochemical detection of vascular endothelial growth factor 165, Anal. Chem. 95 (2023) 16392–16397.
[113] Q.J. Jia, Y.P. Zhang, M.F. Wang, M.H. Wang, J.Y. Tian, S. Zhang, L.H. He, Z. H. Zhang, M. Du, Near-infrared light-assisted dual-modal photoelectrochemical and photo-fuel-cell-driven self-powered biosensor for detection of miRNA-21 in living cancer cells, Microchem. J. 194 (2023) 109292.
[114] W.S. Kong, T.R. Liu, X.X. Meng, P.F. Dong, J.P. Lei, H.X. Ju, Intrareticular energy transfer in dual-photosensitized metal-organic frameworks to enhance photoelectrochemical performance, J. Am. Chem. Soc. 147 (2025) 24976–24983.
[115] X.J. Liu, Y.C. Zhao, F. Li, Nucleic acid-functionalized metal-organic framework for ultrasensitive immobilization-free photoelectrochemical biosensing, Biosens. Bioelectron. 173 (2021) 112832.
[116] L. Zhang, F.Z. Chen, H.D. Sun, R.Z. Meng, Q.S. Zeng, X.X. Wang, H. Zhou, Stimulus-responsive metal-organic framework signal-reporting system for photoelectrochemical and fluorescent dual-mode detection of ATP, ACS Appl. Mater. Interfaces 14 (2022) 46103–46111.
[117] A.P. Côté, A.I. Benin, N.W. Ockwig, M. O'Keeffe, A.J. Matzger, O.M. Yaghi, Porous, crystalline, covalent organic frameworks, Science 310 (2005) 1166–1170.
[118] M.C. Feng, C.Y. Xing, Y.H. Jin, X. Feng, Y.Y. Zhang, B. Wang, Reticular chemistry for enhancing bioentity stability and functional performance, J. Am. Chem. Soc. 146 (2024) 32883–32905.
[119] H. Chen, H.S. Jena, X. Feng, K. Leus, P. Van Der Voort, Engineering covalent organic frameworks as heterogeneous photocatalysts for organic transformations, Angew. Chem. Int. Ed. 61 (2022) e202204938.
[120] X. Zhang, K.N. Chi, D.L. Li, Y. Deng, Y.C. Ma, Q.Q. Xu, R. Hu, Y.H. Yang, 2D-porphrinic covalent organic framework-based aptasensor with enhanced photoelectrochemical response for the detection of c-reactive protein, Biosens. Bioelectron. 129 (2019) 64–71.
[121] H.M. Liu, C.H. Li, L.N. Wang, L.C. Fang, H. Huang, J. Deng, Y. Hu, M.M. Li, X. P. Ran, L.L. Li, J.S. Zheng, Photoelectrochemical sensor based on AuNPs@WO_3@TpPa-1-COF for quantification of DNA methylation levels, Microchim. Acta 191 (2024) 167.
[122] X.X. Yuan, W.C. Geng, J.Y. Ji, Z.Y. Yan, J.R. Wei, Y.J. Wu, R.Y. Yang, CRISPR/Cas13a-programmed CuNCs and Z-scheme T-COF/Ag_2S for photoelectrochemical biosensing of circRNA, ACS Sensors 10 (2025) 1270–1279.
[123] Z.L. He, J. Zhang, X. Li, S.N. Guan, M.C. Dai, S.G. Wang, 1D/2D heterostructured photocatalysts: from design and unique properties to their environmental applications, Small 16 (2020) 2005051.
[124] R.Y. Liu, Z.H. Yu, R. Zhang, J. Xiong, Y.N. Qiao, X.Z. Liu, X.B. Lu, Hollow nanoreactors for controlled photocatalytic behaviors: fundamental theory, structure-performance relationship, and catalytic advantages, Small 20 (2024) 2308142.
[125] E.C. Welch, J.M. Powell, T.B. Clevinger, A.E. Fairman, A. Shukla, Advances in biosensors and diagnostic technologies using nanostructures and nanomaterials, Adv. Funct. Mater. 31 (2021) 2104126.
[126] C. Daulbayev, F. Sultanov, B. Bakbolat, O. Daulbayev, 0D, 1D and 2D nanomaterials for visible photoelectrochemical water splitting. A review, Int. J. Hydrogen Energy 45 (2020) 33325–33342.
[127] S. Odabasi Lee, S.K. Lakhera, K.J. Yong, Strategies to enhance interfacial spatial charge separation for high-efficiency photocatalytic overall water-splitting: a review, Adv. Energy Sustainability Res. 4 (2023) 2300130.
[128] G.Q. Zhang, C.D. Sewell, P.X. Zhang, H.W. Mi, Z.Q. Lin, Nanostructured photocatalysts for nitrogen fixation, Nano Energy 71 (2020) 104645.
[129] D. Zhao, X. Pan, J.H. Zhao, Z. Shen, R. Rong, B.J. Fang, S. Zhang, H.F. Guo, N. Y. Yuan, J.N. Ding, A biosensor based on TiO_2/Sb_2S_3 nanorod array for visible-light induced photoelectrochemical detection of miRNA-155, Microchem. J. 213 (2025) 113731.
[130] Y. Jia, R. Xu, K. Xu, S.F. Wang, X. Ren, N. Zhang, D. Wu, H.M. Ma, Y.Y. Li, Q. Wei, Ternary Z-scheme ag-embedded TiO2-Ag2S nanojunction as a novel photoelectrochemical converter for CD44 detection, Anal. Chem. 94 (2022) 11713–11720.
[131] L. Ge, Y.H. Xu, L.J. Ding, F.H. You, Q. Liu, K. Wang, Perovskite-type BiFeO3/ultrathin graphite-like carbon nitride nanosheets p-n heterojunction: boosted visible-light-driven photoelectrochemical activity for fabricating ampicillin aptasensor, Biosens. Bioelectron. 124–125 (2019) 33–39.
[132] D.L. Zheng, M. Chen, J.J. Peng, J.Y. Chen, T.F. Chen, Y.W. Chen, L.J. Huang, W. H. Gao, An enhanced photoelectrochemical biosensor for colitoxin DNA based on HKUST-1/TiO_2 and derived HKUST-CuO/TiO_2 heterogeneous composites, Microchim. Acta 188 (2021) 328.
[133] Y. Zi, Y. Hu, J.M. Pu, M.K. Wang, W.C. Huang, Recent progress in interface engineering of nanostructures for photoelectrochemical energy harvesting applications, Small 19 (2023) 2208274.
[134] P. Zhang, X.W. Lou, Design of heterostructured hollow photocatalysts for solar-to-chemical energy conversion, Adv. Mater. 31 (2019) 1900281.
[135] D.L. Zheng, J.Y. Yang, Z.Y. Zheng, M.X. Peng, J.Y. Chen, Y.W. Chen, W.H. Gao, A highly sensitive photoelectrochemical biosensor for CEA analysis based on hollow NiS@NiO/TiO_2 composite with typal p-n heterostructure, Talanta 246 (2022) 123523.
[136] Y.T. Zhou, S.Z. Lv, X.Y. Wang, L.Y. Kong, S. Bi, Biometric photoelectrochemical-visual multimodal biosensor based on 3D hollow HCdS@Au nanospheres coupled with target-induced ion exchange reaction for antigen detection, Anal. Chem. 94 (2022) 14492–14501.
[137] H. Ali, Z. Ajmal, A.Y.A. Alzahrani, M.H. Al Mughram, A.M. Abu-Dief, R. Al-Faze, H.M.A. Hassan, S.R. Al-Mhyawi, Y. Al-Hadeethi, Y. Orooji, S.R. Guo, A. Hayat, Defect-driven innovations in photocatalysts: pathways to enhanced photocatalytic applications, InfoMat 7 (2025) e70040.
[138] B.H. Zhang, X.Y. Jian, Z.Q. An, X.T. Yang, H.J. Chen, C.Z. Lu, M.J. Li, L.H. Guo, A colorimetric and photocurrent-polarity-switching photoelectrochemical dual-mode biosensor for the ultrasensitive detection of DNA damage biomarker and rapid screening of genotoxic chemicals, Biosens. Bioelectron. 279 (2025) 117396.
[139] J.J. Zhang, Y.Z. Ning, G.F. Jie, Z. Zong, F. Chai, A dual-mode portable biosensor based on photothermal-pyroelectric-electrochromic effects for versatile detection of enrofloxacin, Biosens. Bioelectron. 290 (2025) 118006.
[140] Y.J. Liu, S.M. Ai, R. Yuan, H.Y. Liu, Defective se-doped In2S3 nanomaterial-based photoelectrochemical biosensor for the ultrasensitive detection of chloramphenicol, Sens. Actuators B 373 (2022) 132705.
[141] Q.Q. Zhang, S.Y. Liu, H.J. Zheng, H.A. Wang, G.Z. Luo, X.H. Zhang, C.C. Du, J. H. Chen, Magnetic photoactive Fe_3O_4@Sb_2S_3 nanospheres assisted homogeneous photoelectrochemical–electrochemical biosensing platform integrating with MOFs-derived bifunctional NPC@Thi nanopolyhedra-mediated dual "signal-on" strategy for protein tyrosine kinase activity, Chem. Eng. J. 476 (2023) 146592.
[142] H.Y. Zou, Y.Y. Zheng, Z.Y. He, C.Y. Deng, J.J. Zhou, PEC/EC dual-signal amplification based on Cd-doped MoS_2 nanoflowers for highly accurate sensing of NT-proBNP in serum samples, Talanta 298 (2026) 129002.
[143] M.L. Cheng, M.L. Huang, H.M. Deng, H.L. Li, R. Yuan, S.P. Wei, The cysteine-induced BiOBr as a novel photoactive material with high photoelectric efficiency for ultrasensitive detection of microRNA, Sens. Actuators B 387 (2023) 214596.
[144] G.F. Wang, L. Li, Y.H. Li, Y.X. Hao, Q.Y. Li, L.N. Zhang, S.G. Ge, P.H. Zhu, H. M. Yang, J.H. Yu, Surface plasmon resonance-enhanced cascaded sensitization effect of CuInSe2/Cu3(BTC)2/Y: ZnO photosensitive structures enabled lab-on-paper photoelectrochemical bioassay, Chem. Eng. J. 476 (2023) 146661.
[145] M.L. Cheng, H.M. Deng, M.L. Huang, H.L. Li, R. Yuan, S.P. Wei, (co, s)-codoped BiOBr as a novel signal probe coupled with LAMP (H+)-pH responsive photoelectrochemistry biosensor for ultrasensitive detection of microRNA, Sens. Actuators B 422 (2025) 136482.
[146] X.K. Niu, Y. Zhao, F. Wang, J.H. Wu, F.L. Qu, W.H. Tan, Ultrasensitive photoelectrochemical biosensor based on novel Z-scheme heterojunctions of zn-defective CdS/ZnS for microRNA assay, Anal. Chem. 93 (2021) 17134–17140.
[147] X.M. Wang, H.P. Li, H.X. Jian, L.P. Liu, H.S. Zeng, J.H. Ai, J. Tang, Robust nCuO modulated by defect engineering enhanced photoelectrochemical biosensor for the detection of miRNA-21, Biosens. Bioelectron. 271 (2025) 117014.
[148] H.L. Wang, L.S. Zhang, Z.G. Chen, J.Q. Hu, S.J. Li, Z.H. Wang, J.S. Liu, X.C. Wang, Semiconductor heterojunction photocatalysts: design, construction, and photocatalytic performances, Chem. Soc. Rev. 43 (2014) 5234.
[149] Z.P. Wang, Z.P. Lin, S.J. Shen, W.W. Zhong, S.W. Cao, Advances in designing heterojunction photocatalytic materials, Chin. J. Catal. 42 (2021) 710–730.
[150] X.H. He, T.H. Kai, P. Ding, Heterojunction photocatalysts for degradation of the tetracycline antibiotic: a review, Environ. Chem. Lett. 19 (2021) 4563–4601.
[151] S.N. Li, W.W. Xu, L.X. Meng, W. Tian, L. Li, Recent progress on semiconductor heterojunction-based photoanodes for photoelectrochemical water splitting, Small Sci. 2 (2022) 2100112.
[152] J.J. Wei, H.B. Li, G.Q. Wang, J.Y. Zheng, A.J. Wang, L.P. Mei, T.J. Zhao, J.J. Feng, Novel ultrasensitive photoelectrochemical cytosensor based on hollow $CdIn_2S_4$/In_2S_3 heterostructured microspheres for HepG2 cells detection and inhibitor screening, Anal. Chem. 94 (2022) 12240–12247.
[153] H.Y. Zou, W.M. Wu, J.J. Zhou, C.Y. Deng, SILAR growth of ZnO NSs/CdS QDs on the optical fiber-based opto-electrode with guided in situ light and its application for the "signal-on" detection of inflammatory cytokine, Anal. Chem. 96 (2024) 5446–5454.
[154] Y.P. Li, G. Adili, G. Liang, Y.H. Ma, J.B. Liu, $CuInS_2$/red phosphorus nanosheet interleaved heterostructures with improved interfacial charge transfer for photoelectrochemical aptasensing, Anal. Chem. 96 (2024) 11985–11996.
[155] H.L. Ding, Y.X. Feng, Y.F. Xu, X.D. Xue, R. Feng, T. Yan, L.G. Yan, Q. Wei, Self-powered photoelectrochemical aptasensor based on MIL-68(in) derived In2O3 hollow nanotubes and ag doped ZnIn2S4 quantum dots for oxytetracycline detection, Talanta 240 (2022) 123153.
[156] H.J. Zheng, S. Zhang, J.F. Yuan, T.T. Qin, T.T. Li, Y.P. Sun, X.Q. Liu, D.K.Y. Wong, Amplified detection signal at a photoelectrochemical aptasensor with a poly (diphenylbutadiene)-BiOBr heterojunction and au-modified CeO2 octahedrons, Biosens. Bioelectron. 197 (2022) 113742.
[157] X.R. Tan, H.H. Yu, B. Liang, M.T. Han, S.G. Ge, L.N. Zhang, L. Li, L. Li, J.H. Yu, A target-driven self-feedback paper-based photoelectrochemical sensing platform for ultrasensitive detection of ochratoxin a with an In2S3/WO3 heterojunction structure, Anal. Chem. 94 (2022) 1705–1712.
[158] Y.R. Xu, H.F. Zhang, Z.L. Zhang, J. Li, F.F. Zong, Y.R. Qi, Y.R. Wang, Y.D. Wu, Novel dual type-II WO_3/g-C_3N_4/Cu_2O-au heterojunction-based photoelectrochemical aptasensor for ultra-sensitive AFB1 detection in astragalus matrix, Microchim. Acta 193 (2025) 35.
[159] L.L. Gao, Y.L. Zhou, L.L. Cao, X.T. Cui, Y.L. Zheng, H.S. Yin, S.Y. Ai, Photoelectrochemical biosensor for histone deacetylase sirt1 detection based on polyaspartic acid-engaged and triggered redox cycling amplification and enhanced photoactivity of $BiVO_4$ by gold nanoparticles and SnS_2, Anal. Chem. 94 (2022) 16936–16944.
[160] S.Y. Meng, Y.Y. Li, N. Dong, S.D. Liu, C. Liu, Q.F. Gong, Z. Chen, K.T. Jiang, X. Li, D. Liu, T.Y. You, Portable visual photoelectrochemical biosensor based on a

MgTi2O5/CdSe heterojunction and reversible electrochromic supercapacitor for dual-modal Cry1Ab protein detection, Anal. Chem. 95 (2023) 18224–18232.
[161] L.B. Mao, H. Liu, L.L. Yao, W. Wen, M.M. Chen, X.H. Zhang, S.F. Wang, Construction of a dual-functional CuO/BiOCl heterojunction for high-efficiently photoelectrochemical biosensing and photoelectrocatalytic degradation of aflatoxin b1, Chem. Eng. J. 429 (2022) 132297.
[162] L.C. Wang, Y.P. Wei, J.S. Chen, X.P. Liu, C.J. Mao, B.K. Jin, A "signal-on" photoelectrochemical biosensor utilizing in-situ synthesis of SnS_2/$MgIn_2S_4$ heterostructures and enzyme-assisted target cycling amplification for the sensitive detection of the mecA gene, Talanta 293 (2025) 128053.
[163] Y.Z. Huang, J.Y. Lv, L.X. Gu, J.J. Tao, Y. Zhao, J.J. Shi, S.L. Jiao, L. Liu, Atomic layer deposition-derived MoS_2/NbS_2 nanoheterojunctions enable high-density quantum dot loading for enhanced signal-on photoelectrochemical detection of cTnI, ACS Appl. Mater. Interfaces 17 (2025) 49020–49028.
[164] L. Wu, J.Y. Dong, L.S. Zhao, A photoelectrochemical sensor for detection of 17β-estradiol using high-response type II heterojunction: implementation of visualization strategy, Sens. Actuators B 378 (2023) 133135.
[165] M. Wang, X.J. Gao, L. Hou, Y.L. Chen, T.R. Lin, A novel split-type photoelectrochemical biosensor based on liposome-induced in situ formation of Bi_2S_3@BiOI/Ag_2S heterojunction for the sensitive detection of CEA, Microchem. J. 200 (2024) 110388.
[166] S.T. Liu, J.S. Chen, X.P. Liu, C.J. Mao, B.K. Jin, A photoelectrochemical biosensor based on b-TiO2/CdS: Eu/Ti3C2 heterojunction for the ultrasensitive detection of miRNA-21, Talanta 253 (2023) 123601.
[167] Z.D. Yin, H.S. Yin, Y.L. Zhou, H.D. Liu, CRISPR/Cas13a-mediated photoelectrochemical-colorimetric dual-mode biosensor for RNA n-acetyltransferase 10 detection based on Bi2O2S/Ag2S and laccase-like nanozyme, Biosens. Bioelectron. 295 (2026) 118298.
[168] F. Mo, J.J. Zhao, Y.J. Du, W. Li, Q. Sun, X.Z. Huang, G.Q. Wu, Y.J. Zhang, Y. F. Shen, In-situ fabrication of BiOI-based single transducer enabling dual photoelectrochemical/colorimetric biosensing, Biosens. Bioelectron. 294 (2026) 118235.
[169] Y.Y. Zhang, T.T. Wu, D.L. Liu, R. Xu, H.M. Ma, Q. Wei, Y. Zhang, Photoelectrochemical immunosensor for the sensitive detection of neuron-specific enolase based on the effect of z-scheme WO3/NiCo2O4 nanoarrays p-n heterojunction, Biosens. Bioelectron. 213 (2022) 114452.
[170] Y. Zhang, Q. Wang, D.M. Liu, Q. Wang, T. Li, Z. Wang, Cu2O-BiOI isotype (p-p) heterojunction: boosted visible-light-driven photoelectrochemical activity for non-enzymatic H2O2 sensing, Appl. Surf. Sci. 521 (2020) 146434.
[171] D. Zhao, C.Y. Geng, X.Q. Liu, X.X. Jin, Z.J. Zhao, Y. Liu, S. Alwarappan, Photoelectrochemical detection of superoxide anions released from mitochondria in HepG2 cells based on the synergistic effect of MnO_2@Co_3O_4 core-shell p-n heterojunction, Biosens. Bioelectron. 237 (2023) 115368.
[172] J. Zhang, Y. Gao, P. Liu, J. Yan, X. Zhang, Y. Xing, W. Song, Charge transfer accelerated by internal electric field of MoS_2 QDs-BiOI p-n heterojunction for high performance cathodic PEC aptasensing, Electrochim. Acta 365 (2021) 137392.
[173] X.Y. Li, H.B. Sun, Y.Y. Xie, Y.S. Liang, X.M. Gong, P.F. Qin, L.B. Jiang, J.Y. Guo, C. Liu, Z.B. Wu, Principles, synthesis and applications of dual z-scheme photocatalysts, Coord. Chem. Rev. 467 (2022) 214596.
[174] C.Q. Zhuang, A.L. Zhang, Y.H. Zhang, H.S. Zhu, W. Zhang, P. Shan, P. Xu, Z.L. Jin, H.W. Huang, S.J. Li, Photocatalytic cocatalysts: classification, structural design and crucial role in various reactions, Coord. Chem. Rev. 542 (2025) 216867.
[175] W.W. Ding, H.H. Yu, J.L. Yin, S.G. Ge, J.H. Yu, C.M. Gao, Engineering atomically precise cobalt charge-transfer bridges for cascade amplification-enhanced photoelectrochemical sensing, Adv. Funct. Mater. 36 (2025) e18134.
[176] A. J. Bard, Photoelectrochemistry and heterogeneous photo-catalysis at semiconductors, J. Photochem 10 (1979) 59.
[177] H. Tada, T. Mitsui, T. Kiyonaga, T. Akita, K. Tanaka, All-solid-state z-scheme in CdS-au-TiO2 three-component nanojunction system, Nat. Mater. 5 (2006) 782–786.
[178] Y.X. Li, R.J. Zeng, W.J. Wang, J.H. Xu, H.X. Gong, L. Li, M.J. Li, D.P. Tang, Size-controlled engineering photoelectrochemical biosensor for human papillomavirus-16 based on CRISPR-Cas12a-induced disassembly of Z-scheme heterojunctions, ACS Sens. 7 (2022) 1593–1601.
[179] X.W. Wang, G. Liu, Z.G. Chen, F. Li, L.Z. Wang, G.Q. Lu, H.M. Cheng, Enhanced photocatalytic hydrogen evolution by prolonging the lifetime of carriers in ZnO/CdS heterostructures, Chem. Commun. 23 (2009) 3452–3454.
[180] J.G. Yu, S.H. Wang, J.X. Low, W. Xiao, Enhanced photocatalytic performance of direct z-scheme g-C3N4-TiO2 photocatalysts for the decomposition of formaldehyde in air, Phys. Chem. Chem. Phys. 15 (2013) 16883.
[181] S. Zhang, J.H. Sun, H.X. Ju, Z-scheme heterojunction of hierarchical Cu_2S/$CdIn_2S_4$ hollow cubes to boost photoelectrochemical performance, Small 20 (2024) 2405712.
[182] J.W. Fu, Q.L. Xu, J.X. Low, C.J. Jiang, J.G. Yu, Ultrathin 2D/2D WO3/g-C3N4 step-scheme h2-production photocatalyst, Appl. Catal. B 243 (2019) 556–565.
[183] Y.K. Liu, C.G. Chen, G. Dawson, J.F. Zhang, C.F. Shao, K. Dai, Organic-inorganic hybrid-based s-scheme heterostructure in solar-to-fuel conversion, J. Mater. Sci. Technol. 233 (2025) 10–37.
[184] C.H. Wang, Y.Y. Zhao, C. Cheng, Q. Li, C.F. Guo, Y. Hu, S-scheme heterojunction photocatalysts: mechanism, challenges and opportunities, Coord. Chem. Rev. 521 (2024) 216177.
[185] L.Y. Zhang, J.J. Zhang, H.G. Yu, J.G. Yu, Emerging s-scheme photocatalyst, Adv. Mater. 34 (2022) 2107668.
[186] X. Yang, X.D. Xiao, Z. Sun, H.R. Mou, H.R. Tao, H.Q. Luo, N.B. Li, Oxygen vacancy-rich SnO_2/$CdIn_2S_4$ heterojunction with self-primed multi-cycle amplification for sensitive ctDNA detection, Sens. Actuators B 425 (2025) 136979.
[187] C.C. Hu, Q.E. Zhang, S.P. Shi, G.Q. Zhao, Y.S. Gao, P. Liu, X.K. Ye, Y. Pan, H.Q. Lv, L.M. Lu, Ti_3C_2-cl-$Bi_{12}O_{17}Cl_2$/$Bi_{12}O_{17}Cl_2$ Mott-Schottky heterojunction with mixed noncovalent/covalent type to boost ultra-sensitive photoelectrochemical sensing of ciprofloxacin, Chem. Eng. J. 527 (2026) 171533.
[188] Z.R. Wen, W.R. Zhu, F.H. You, R.S. Yuan, L.J. Ding, N. Hao, J. Wei, K. Wang, Ultrasensitive photoelectrochemical aptasensor for carbendazim detection based on in-situ constructing schottky junction via photoreducing pd nanoparticles onto CdS microsphere, Biosens. Bioelectron. 203 (2022) 114036.
[189] M. Chen, H. Meng, F.J. Mo, J. Guo, Y.Z. Fu, An electron donor-acceptor organic photoactive composite with schottky heterojunction induced photoelectrochemical immunoassay, Biosens. Bioelectron. 191 (2021) 113475.
[190] P. Miao, B. Wang, G.X. Zheng, W.S. Wang, Y.F. Lv, J. Zhang, M. Yan, CRISPR/Cas13a-mediated dual-modal biosensing platform based on the Zn0.5Cd0.5S/Ti3C2 schottky heterojunction for the sensitive detection of miRNAs-21, Sens. Actuators B 400 (2024) 134829.
[191] Y.P. Tu, H.H. Wang, D. Long, R. Yuan, Y.Q. Chai, Highly sensitive photoelectrochemical biosensor based on au nanoparticles sensitized zinc selenide quantum dots for DNA detection, Sens. Actuators B 357 (2022) 131255.
[192] C. Ye, M.Q. Wang, H.Q. Luo, N.B. Li, Label-free photoelectrochemical "off-on" platform coupled with g-wire-enhanced strategy for highly sensitive microRNA sensing in cancer cells, Anal. Chem. 89 (2017) 11697–11702.
[193] W.Q. Yu, F.J. Mo, J. Guo, Y.Q. Yang, Y.S. Jin, Y.Z. Fu, Ultrasensitive microRNA photoelectric assay based on a mimosa-like CdS-NiS/au schottky junction, Anal. Chem. 95 (2023) 12097–12103.
[194] L. Zhang, Y. Zhang, S.Y. Zhao, W.W. Ma, Z.Y. Feng, Y.F. Wu, Y.L. Wang, D.Z. Li, Q. Liu, Z.T. Gu, Research progress on photoelectrochemical immunosensors for serum markers of thoracic malignancy: a review, Microchem. J. 215 (2025) 114242.
[195] L.P. Zhao, L.S. Li, Y. Zhao, C. Zhu, R.Q. Yang, M.Q. Fang, Y.X. Luan, Aptamer-based point-of-care-testing for small molecule targets: from aptamers to aptasensors, devices and applications, Trends Anal. Chem. 169 (2023) 117408.
[196] R. Napit, S.K. Jaysawal, R. Chowdhury, J. Catague, H. Melke, C.V. Pham, H. Xu, L. Jia, J. Lin, Y.C. Hou, W. Duan, Aptasensors and advancement in molecular recognition technology, Adv. Mater. Technol. 10 (2025) 2400504.
[197] B.H. Zhang, Z.Q. An, M.J. Li, L.H. Guo, Synthesis, functionalization and photoelectrochemical immunosensing application of WO_3-based semiconductor materials, Trends Anal. Chem. 165 (2023) 117149.
[198] Q.X. Zhang, X.W. Liu, H.R. Wang, Q. Liu, Q.Y. Liu, X.X. Zhang, Photoelectrochemical thrombin biosensor based on perylene-3,4,9,10-tetracarboxylic acid and au co-functionalized ZnO nanorods with signal-off quenching effect of ag@Ag2S, Analyst 146 (2021) 855–863.
[199] J. Gao, Y.F. Ding, K. Yan, J.D. Zhang, A near-infrared light-driven photoelectrochemical aptasensing platform for adenosine triphosphate detection based on yb-doped Bi2S3 nanorods, J. Mater. Chem. B 10 (2022) 3524–3530.
[200] P. Miao, C.M. Gao, M.J. Hao, C.C. Zhang, Z.J. Li, S.G. Ge, Z.L. Song, J. Zhang, M. Yan, J.H. Yu, Ultrasensitive DNA detection based on inorganic-organic nanocomposite cosensitization and G-Quadruplex/hemin catalysis for signal amplification, ACS Appl. Mater. Interfaces 12 (2020) 42604–42611.
[201] J.H. Zhu, H.W. Gou, T.J. Zhao, L.P. Mei, A.J. Wang, J.J. Feng, Ultrasensitive photoelectrochemical aptasensor for detecting telomerase activity based on Ag2S/ag decorated ZnIn2S4/C3N4 3D/2D z-scheme heterostructures and amplified by au/Cu2+−boron-nitride nanozyme, Biosens. Bioelectron. 203 (2022) 114048.
[202] G. Wang, L. Li, Y. Li, Y. Hao, Q. Li, L. Zhang, S. Ge, P. Zhu, H. Yang, J. Yu, Surface plasmon resonance-enhanced cascaded sensitization effect of CuInSe2/Cu3(BTC)2/Y: ZnO photosensitive structures enabled lab-on-paper photoelectrochemical bioassay, Chem. Eng. J. 476 (2023) 146661.
[203] Y.X. Wen, M. Qing, S.L. Chen, H.Q. Luo, N.B. Li, Y-type DNA structure stabilized p-type CuS quantum dots to quench photocurrent of ternary heterostructure for sensitive photoelectrochemical detection of miRNA, Sens. Actuators B 329 (2021) 129257.
[204] L.D. Yu, Y.X. Wen, X.Y. Zhang, N.B. Li, H.Q. Luo, Signal-off photoelectrochemical determination of miRNA-21 using aptamer-modified In_2O_3@Cu_2MoS_4 nanocomposite, Microchim. Acta 187 (2020) 561.
[205] W.W. Zhao, J. Wang, J.J. Xu, H.Y. Chen, Energy transfer between CdS quantum dots and au nanoparticles in photoelectrochemical detection, Chem. Commun. 47 (2011) 10990–10992.
[206] X.M. Shi, L.P. Mei, Q. Wang, W.W. Zhao, J.J. Xu, H.Y. Chen, Energy transfer between semiconducting polymer dots and gold nanoparticles in a photoelectrochemical system: a case application for cathodic bioanalysis, Anal. Chem. 90 (2018) 4277–4281.
[207] S. Zhang, H.J. Zheng, Y.P. Sun, F. Li, T.T. Li, X.Q. Liu, Y.M. Zhou, W.W. Chen, H. X. Ju, Oxygen vacancies enhanced photoelectrochemical aptasensing of 2, 3′, 5, 5′-tetrachlorobiphenyl amplified with Ag_3VO_4 nanoparticle-TiO_2 nanotube array heterostructure, Biosens. Bioelectron. 167 (2020) 112477.
[208] Y. Zhan, J. Tang, D. Huang, L.N. Zou, B.X. Ye, Quenched sandwich-type photoelectrochemical aptasensor for protein detection based on exciton energy transfer, Talanta 198 (2019) 302–309.
[209] J. Yang, F. Luo, J. Wang, B. Qiu, J. Shen, L. Zhang, Z.Y. Lin, Ultrasensitive photoelectrochemical biosensor for microRNA-155 based on energy transfer between au nanocages and red emission carbon dot-assembled nanosheets coupled with the duplex-specific nuclease enzyme-assisted target recycling strategy, Anal. Chem. 94 (2021) 1482–1490.

[210] Y.M. Fu, B.H. Fan, S.Z. Chang, D.Y. Guo, F.X. Wang, Q.H. Pan, An ultrasensitive photoelectrochemical assay for Tumor Necrosis Factor-alpha based on hollow CdS cubes as a signal generator and NiCo2O4-au as a signal extinguisher, Analyst 148 (2023) 4746–4752.
[211] M.J. Hao, P. Miao, Y. Wang, W.S. Wang, S.G. Ge, X.Y. Yu, X.X. Hu, B.Y. Ding, J. Zhang, M. Yan, Near-infrared light-initiated photoelectrochemical biosensor based on upconversion nanorods for immobilization-free miRNA detection with double signal amplification, Anal. Chem. 93 (2021) 11251–11258.
[212] X.P. Liu, Y.P. Wei, J.S. Chen, C.J. Mao, B.K. Jin, A photoelectrochemical biosensor based on an MXene-based Ti3C2Tx/g-C3N4/CdSe heterojunction and AgInS2 amplification for the detection of cyfra21-1, Microchem. J. 216 (2025) 114578.
[213] H.M.L. Cai, J. Sun, Z.C. Ma, J.W. Di, A "turn-on" photoelectrochemical DNA biosensor based on charge transfer between $BiVO_4$ and gold nanoparticles, J. Electroanal. Chem. 948 (2023) 117822.
[214] Y.C. Zhao, J.Z. Xiang, H. Cheng, X.J. Liu, F. Li, Flexible photoelectrochemical biosensor for ultrasensitive microRNA detection based on concatenated multiplex signal amplification, Biosens. Bioelectron. 194 (2021) 113581.
[215] Y. Zhong, Z.W. Xu, Z.J. Cheng, A.L. Liu, Y. Lei, A y-shape-structured photoelectrochemical biosensor based on Bi4NbO8Cl/TiO2 heterojunction and enzyme-mediated electrocatalysis for sensitive and selective determination of microRNA in serum, Microchem. J. 214 (2025) 113954.
[216] H.H. Yu, X.R. Tan, L.N. Zhang, H.M. Yang, P.H. Zhu, Z. Yan, C.M. Gao, J.H. Yu, Metal-organic framework-enabled surface state passivation integrating with single-nuclease-propelled multistage amplification for ultrasensitive lab-on-paper photoelectrochemical biosensing, Chem. Eng. J. 450 (2022) 137955.
[217] Y.X. Qiao, S. Qiao, F.Y. Su, W.M. Li, Y. Wang, Y. Li, D.D. Fan, Incorporation of sensitization of photoactive materials and enzyme-assisted dual sensitivity amplification for photoelectrochemical detection of microRNA in human liver cancer, Chem. Eng. J. 524 (2025) 169764.
[218] J.R. Luo, Q. Zeng, S.P. Liu, Q.Y. Wei, Z.X. Wang, M.H. Yang, Y.P. Zou, L.M. Lu, Highly sensitive photoelectrochemical sensing platform based on PM6: Y6 p-n heterojunction for detection of MCF-7 cells, Sens. Actuators B 363 (2022) 131814.
[219] Y.Y. Wei, S.H. Wu, Q.M. Wang, J.J. Sun, A novel split-type photoelectrochemical biosensor based on double-strand specific nuclease-assisted cycle amplification coupled with plasmonic ag enhanced BiVO4 performance for sensitive detection of microRNA-155, Sens. Actuators B 369 (2022) 132251.
[220] L.L. Lu, R.J. Zeng, Q.Y. Lin, X. Huang, D.P. Tang, Cation exchange reaction-mediated photothermal and polarity-switchable photoelectrochemical dual-readout biosensor, Anal. Chem. 95 (2023) 16335–16342.
[221] Y.M. Fu, K. Zou, M.Y. Liu, X.H. Zhang, C.C. Du, J.H. Chen, Highly selective and sensitive photoelectrochemical sensing platform for VEGF165 assay based on the switching of photocurrent polarity of CdS QDs by porous Cu_2O-CuO flower, Anal. Chem. 92 (2020) 1189–1196.
[222] R.J. Zeng, J.H. Xu, T.K. Liang, M.J. Li, D.P. Tang, Photocurrent-polarity-switching photoelectrochemical biosensor for switching spatial distance electroactive tags, ACS Sens. 8 (2023) 317–325.
[223] L.N. Zhang, L. Zhang, D.D. Liu, S.J. Wang, R.F. Liu, L.F. Zhu, C.X. Li, L. Xie, S. G. Ge, J. Wang, Exponential amplification reaction assisted CRISPR/Cas12a target-induced polarity switching photoelectrochemical biosensor for miRNA-622 detection, Sens. Actuators B 436 (2025) 137723.
[224] Y.L. Li, L. Liu, H.C. Han, X.X. Yuan, J.Y. Ji, L.S. Xue, Y.J. Wu, R.Y. Yang, A signal-switchable photoelectrochemical biosensor for ultrasensitive detection of long non-coding RNA in cancer cells, Talanta 273 (2024) 125878.
[225] X.X. Jiang, C.Q. Bao, J.W. Liu, Y. Lu, X. Chen, M.H. Yang, X.Q. Li, Photocurrent polarity reversal induced by $CuBi_2O_4$ for sensitive photoelectrochemical detection of circulating tumor cells, Microchim. Acta 192 (2025) 815.
[226] Y.M. Fu, Q. Yu, Q.Q. Zhang, X.H. Zhang, C.C. Du, J.H. Chen, A photocurrent-polarity-switching biosensor for highly selective assay of mucin 1 based on target-induced hemin transfer from ZrO2 hollow spheres to g-quadruplex nanowires, Biosens. Bioelectron. 192 (2021) 113547.
[227] J.H. Xu, J.X. Zhang, R.J. Zeng, L. Li, M.J. Li, D.P. Tang, Target-induced photocurrent-polarity-switching photoelectrochemical aptasensor with gold nanoparticle-$ZnIn_2S_4$ nanohybrids for the quantification of 8-hydroxy-2′-deoxyguanosine, Sens. Actuators B 368 (2022) 132141.
[228] W. Huang, F.P. Liu, L.G. Geng, S.L. Zhao, F.G. Ye, Photoelectrochemical biosensing platform based on switch of photocurrent polarity of CdS/Ni-CAT nanorod arrays by au@Cu_2O for highly selective and sensitive CEA detection, Talanta 286 (2025) 127489.
[229] P. Wu, X.D. Hou, J.J. Xu, H.Y. Chen, Ratiometric fluorescence, electrochemiluminescence, and photoelectrochemical chemo/biosensing based on semiconductor quantum dots, Nanoscale 8 (2016) 8427–8442.
[230] Q. Hao, X.N. Shan, J.P. Lei, Y. Zang, Q.H. Yang, H.X. Ju, A wavelength-resolved ratiometric photoelectrochemical technique: design and sensing applications, Chem. Sci. 7 (2016) 774–780.
[231] H.M. Yang, M.S. Hu, Z.L. Li, P.N. Zhao, L. Xie, X.R. Song, J.H. Yu, Donor/acceptor-induced ratiometric photoelectrochemical paper analytical device with a hollow double-hydrophilic-walls channel for microRNA quantification, Anal. Chem. 91 (2019) 14577–14585.
[232] Q. Zhang, Y. Sun, L. Yu, X. Gao, Y. Huang, X. Sun, Y.L. Pak, Y.R. Guo, Y. Sun, Z. Wang, J.B. Song, A portable photoelectrochemical aptasensor based on voltage-resolved dual-signal output for the determination of chloramphenicol, J. Hazard. Mater. 490 (2025) 137748.
[233] Z.L. Qiu, J. Shu, J.F. Liu, D.P. Tang, Dual-channel photoelectrochemical ratiometric aptasensor with up-converting nanocrystals using spatial-resolved technique on homemade 3D printed device, Anal. Chem. 91 (2019) 1260–1268.
[234] Y.N. Zheng, W.B. Liang, C.Y. Xiong, Y. Zhuo, Y.Q. Chai, R. Yuan, Universal ratiometric photoelectrochemical bioassay with target-nucleotide transduction-amplification and electron-transfer tunneling distance regulation strategies for ultrasensitive determination of microRNA in cells, Anal. Chem. 89 (2017) 9445–9451.
[235] T.T. Wang, Y.Q. Ran, L. Shi, F.Q. Zhao, B.Z. Zeng, A universal dual-channel ratiometric photoelectrochemical sensing platform with integrated ionic liquid-sensitized In_2S_3@$BiOBr_{0.8}I_{0.2}$/PEDOT photoanode and Cu@Cu_2O photocathode, Chem. Eng. J. 486 (2024) 150314.
[236] J. Wei, Z. Yan, M. Mei, S. Chen, W. Geng, Z. Yu, R. Yang, Machine learning-assisted BMOFs-derived 1D $NiCo_2O_4$ nanozyme photoelectrochemical detection of RBP4 for type 2 diabetes diagnosis, Chem. Eng. J. 524 (2025) 169192.
[237] F. Yan, R. Bai, J. Huang, X. Bian, Y. Fu, Machine learning-assisted carbon dots synthesis and analysis: state of the art and future directions, TrAC Trends Anal. Chem. 184 (2025) 118141.
[238] F. Cui, Y. Yue, Y. Zhang, Z. Zhang, H.S. Zhou, Advancing biosensors with machine learning, ACS Sens. 5 (2020) 3346–3364.
[239] X. Ma, Z. Yin, Z. Cao, B. Shi, X. Yan, D. Wu, Y. Wang, C. Dai, M. Hong, Machine learning assisted photocurrent wavelength classification in a self-powered broadband photoelectrochemical photodetector based on $Bi_2Te_{0.6}Se_{2.4}$/$MoSe_2$ heterojunctions, Chem. Eng. J. 524 (2025) 169645.
[240] R. Mohammadzadeh kakhki, M. Mohammadpoor, Machine learning-driven approaches for synthesizing carbon dots and their applications in photoelectrochemical sensors, Inorg. Chem. Commun. 159 (2024) 111859.
[241] W. Geng, J. Ji, Z. Yan, F. Wu, J. Chang, J. Wei, M. Mei, S. Chen, F. Wang, R. Yang, Machine learning-assisted photoelectrochemical biosensor based on DNA-AgNCs nanowires for exosomal lncRNA intelligent diagnosis, Anal. Chim. Acta 1384 (2026) 344981.
[242] W. Geng, X. Yuan, J. Wei, Z. Yan, M. Mei, S. Chen, R. Yang, Machine learning-assisted renewable and polarity-switchable photoelectrochemical biosensor for circRNA intelligent diagnosis, Biosens. Bioelectron. 294 (2026) 118197.

Si Zhang received her B.S. degree in Chemistry from Zhongyuan Institute of Science and Technology in 2018 and M.S. degree in Analytical Chemistry from Henan University in 2021. Now, she is studying in Prof. Huangxian Ju's group at the School of Chemistry, Nanjing University, China. Her research interests focus on photoactive materials and photoelectrochemical aptasensors.

Zihan Huang received her B.S. degree in Chemistry from Shangqiu Normal University in 2021 and M.S. degree in Analytical Chemistry from Liaoning Petrochemical University in 2024, Now, she is studying in Prof. Huangxian Ju's group at the School of Chemistry, Nanjing University, China.

Jiahui Sun: received her B.S. degree in Chemistry in 2018 and M.S. degree in Analytical Chemistry in 2021, both from Anhui Normal University. Now, she is studying in Prof. Huangxian Ju's group at the School of Chemistry, Nanjing University, China.

Huangxian Ju received his BS, MS and Ph.D. degrees from Nanjing University during 1982–1992, and became an associate and full professor of Nanjing University in 1993 and 1999. He was a postdoc in Montreal University (Canada) from 1996 to 1997. He is currently the director of State Key Laboratory of Analytical Chemistry for Life Science. His research interests focus on analytical biochemistry, biosensing and molecular diagnosis. He has authored 112 patents with 67 patents approved, 7 English books, 7 Chinese books and 20 chapters, and published 1021 papers in different journals with h-index of 114 and >55000 citations (Google Scholar h-index 125 with more than 61000 citations).